The Astrophysical Journal, 600:804–827, 2004 January 10

ON THE FLUX OF EXTRASOLAR DUST IN EARTH'S ATMOSPHERE

N. Murray,[1] Joseph C. Weingartner,[2] and C. Capobianco
Canadian Institute for Theoretical Astrophysics, 60 St. George Street, University of Toronto, Toronto, ON M5S 3H8, Canada; murray@cita.utoronto.ca, weingart@cita.utoronto.ca
Received 2003 June 30; accepted 2003 September 29

ABSTRACT

Micron-size extrasolar dust particles have been convincingly detected by satellites. Larger extrasolar meteoroids (5–35 μm) have most likely been detected by ground-based radar at Arecibo and New Zealand. We present estimates of the minimum detectable particle sizes and the collecting areas for both radar systems. We show that particles larger than $\sim$10 μm can propagate for tens of parsecs through the interstellar medium, opening up the possibility that ground-based radar systems can detect AGB stars, young stellar objects such as T Tauri stars, and debris disks around Vega-like stars. We provide analytical and numerical estimates of the ejection velocity in the case of a debris disk interacting with a Jupiter-mass planet. We give rough estimates of the flux of large micrometeoroids from all three classes of sources. Current radar systems are unlikely to detect significant numbers of meteors from debris disks such as β Pictoris. However, we suggest improvements to radar systems that should allow for the detection of multiple examples of all three classes.

Subject headings: dust, extinction — planetary systems: protoplanetary disks

1. INTRODUCTION

In astronomy, as in everyday life, most of our information comes to us in the form of electromagnetic radiation. Some astronomical systems also emit solid particles, which could yield valuable information if detected. The dust detectors on the *Ulysses* and *Galileo* spacecraft have yielded preliminary information on the flux of interstellar grains passing through the solar system (Frisch et al. 1999; Landgraf et al. 2000). Because of the limited area of the collecting surfaces, of the order of 200 cm^2, these authors were unable to report fluxes for grains with masses $\gtrsim 10^{-10}$ g. The low-mass grains that were detected cannot be traced to their point of origin, since interstellar influences (e.g., gas drag, radiation pressure, magnetic fields) rapidly adjust their velocities.

Particle fluxes probably decline dramatically as the grain mass increases, necessitating dust detectors with much larger collecting areas. Meteor-tracking radar facilities can be used to detect grains originating beyond the solar system, if the grain's initial velocity can be inferred with sufficient accuracy. The effective collecting area in this case could be $\gtrsim 10^4$ km^2.

Recently, Baggaley and coworkers reported the detection of extrasolar grains using the Advanced Meteor Orbit Radar (AMOR; Baggaley et al. 1994; Baggaley 2000). Baggaley (2000) finds a "discrete source" with an angular diameter of $\sim 30^\circ$, which he tentatively associates with β Pic. Inspection of his Figure 2 suggests the presence of a broad, bandlike feature as well. Baggaley does not provide any estimate of the particle fluxes.

Our goal here is to identify likely sources of extrasolar grains and estimate expected fluxes at Earth, as a function of the grain size. We consider three types of objects that could potentially yield significant fluxes: young main-sequence stars, asymptotic giant branch (AGB) stars, and young stellar objects (YSOs).

For a given source of interest, the flux at Earth depends on the following three factors:

1. The "dust luminosity" of the source, i.e., the rate at which grains are emitted. We also need to know whether or not the emission is isotropic. If not, then we need to know the orientation of the source.
2. The distance between the source (at the time when the grains were ejected) and the Sun (now).
3. The probability that the grain survives the trip and is not deflected on its way. Although deflected grains can be detected at Earth and will contribute to the general dust background, they do not reveal their source.

Define the "specific dust luminosity" $L_{v,a}(t, v_{\rm ej}, a)$ by

$$L(t) = \int dv_{\rm ej}\, da\, L_{v,a}\left(t, v_{\rm ej}, a\right), \tag{1}$$

where t is the age of the source, $L(t)$ is the dust luminosity, $v_{\rm ej}$ is the speed at which grains are ejected, and a is the grain radius.[3] In order to calculate the dust flux at Earth, it is most convenient to consider the reference frame in which the source is stationary. We assume that, in this frame, large grains simply travel radially outward; i.e., we ignore the Galactic potential and gravitational interactions with individual stars, as well as any other influences that could deflect the grains (see § 3.2). The number density of grains at distance d from the source is given by $n(t, d) = \int dv_{\rm ej}\, da\, n_{v,a}(t, v_{\rm ej}, a, d)$, where

$$n_{v,a}\left(t, v_{\rm ej}, a, d\right) = \frac{L_{v,a}\left(v_{\rm ej}, a, t_{\rm ej} = t - d/v_{\rm ej}\right)}{4\pi d^2 v_{\rm ej}} f_{\rm beam} f_{\rm survive}\left(v_{\rm ej}, a, d\right). \tag{2}$$

[1] Canada Research Chair in Astrophysics.
[2] Current address: Department of Physics and Astronomy, George Mason University, 4400 University Drive, MSN 3F3, Fairfax, VA 22030.
[3] Throughout this paper we make the simplifying assumption that the grains are spheres.

Here $t_{\rm ej}$ is the age of the source when the grains are ejected. The factor $f_{\rm beam}$ accounts for anisotropic emission from the source (we assume that it is independent of $v_{\rm ej}$ and a), and $f_{\rm survive}(v_{\rm ej}, a, d)$ is the fraction of the grains that survive the trip out to distance d without being destroyed or significantly deflected. The particle flux at Earth at the present time is given by $F(t) = \int dv_{\rm ej}\, da\, F_{v,a}(t, v_{\rm ej}, a, d)$, where

$$\begin{aligned} F_{v,a}\left(t, v_{\rm ej}, a, d\right) &= n_{v,a}\left(t, v_{\rm ej}, a, d\right) v_{d,\odot} \\ &= \frac{L_{v,a}\left(v_{\rm ej}, a, t_{\rm ej} = t - d/v_{\rm ej}\right)}{4\pi d^2} \frac{v_{d,\odot}}{v_{\rm ej}} \\ &\quad \times f_{\rm beam} f_{\rm survive}\left(v_{\rm ej}, a, d\right). \end{aligned} \tag{3}$$

The velocity of the dust grain with respect to the Sun is given by

$$\boldsymbol{v}_{d,\odot} = \boldsymbol{v}_{*,\odot} - v_{\rm ej}\hat{\boldsymbol{r}}_{*,\odot}, \tag{4}$$

where $\boldsymbol{v}_{*,\odot}$ is the velocity of the source with respect to the Sun and $\hat{\boldsymbol{r}}_{*,\odot}$ is the unit vector pointing from the Sun to the source.

In § 2 we estimate the limiting particle flux that could potentially be detected with radar facilities. In § 3 we consider the mechanisms that can prevent a grain from reaching us and estimate the (size-dependent) distance that a grain can travel and still reveal its source. We estimate observable dust fluxes from young main-sequence stars, AGB stars, and YSOs in §§ 4, 5, and 6, respectively. We discuss our results in § 7 and summarize our conclusions in § 8.

2. DETECTABLE FLUXES

2.1. *Satellite Measured Fluxes*

There have been several claimed detections of extrasolar grains, from both satellite detectors and ground-based radar. The most convincing detections are those of the *Ulysses* and *Galileo* satellites. Frisch et al. (1999) and Landgraf et al. (2000) show that the flux of $m \approx 6 \times 10^{-13}$ g extrasolar particles is given by $mf_m \approx 10^{-9}$ cm^{-2} s^{-1}. Here $f_m\, dm$ is the flux of particles with masses between m and $m + dm$.[4] At the low-mass end of the mass distribution (below $m \approx 6 \times 10^{-13}$ g) the particles are subject to strong perturbations from the solar wind and its associated magnetic field, so that the measured flux is not representative of the flux of small particles outside the heliosphere. Above $m \approx 6 \times 10^{-13}$ g, they find $mf_m \propto m^{-1.1}$; there are roughly equal masses of particles in every logarithmic mass bin.

For purposes of extrapolation we occasionally assume that the cumulative flux of interstellar particles of mass m is

$$f_{\log_{10} m} \approx 3 \times 10^{-9} \left(\frac{6 \times 10^{-13}\ {\rm g}}{m}\right)^{1.1}\ {\rm cm}^{-2}\ {\rm s}^{-1}, \tag{5}$$

for $m > 6 \times 10^{-13}$ g.

We employ two other differential fluxes. The first is f_a, where $f_a\, da$ is the flux of particles with radii between a and $a + da$; f_a has units cm^{-2} s^{-1} cm^{-1}. In many cases one assumes that f_a follows a power-law distribution, $f_a \propto a^{-\gamma}$. This corresponds to $f_m \propto m^{-\alpha}$, with $\alpha = (\gamma + 2)/3$. We also use the differential mass flux, $m^2 f_m$, with units g cm^{-2} s^{-1}.

In the asteroid literature one encounters the Dohnanyi (1969) law, $f_m \propto m^{-\alpha}$, with $\alpha = 11/6$, corresponding to $\gamma = 7/2$. The Dohnanyi law represents a singular, steady state solution to a set of equations describing a closed system of colliding bodies. Asteroids do not follow this relation (Ivezić et al. 2001). The same scaling appears in the interstellar dust literature, in the MRN dust model (Mathis, Rumpl, & Nordsieck 1977). In these models the mass in large particles diverges in proportion to $a^{1/2}$, or as $m^{1/6}$. The observed scaling (eq. [5]) is $\alpha \approx 2.1$, slightly larger than the Dohnanyi value, so that the mass in large particles is finite. We note that particles in debris disks or in the outflows of AGB stars need not be distributed according to either law; in fact, the findings below suggest that they are not well described by a power law with $\gamma = 7/2$.

2.2. *Radar Fluxes*

Ground-based radar at Arecibo (Meisel, Janches, & Mathews 2002a) and in New Zealand (AMOR; Taylor, Baggaley, & Steel 1996; Baggaley 2000) have also reported detections of extrasolar meteors. When a meteoroid enters Earth's atmosphere, air molecules ablate and ionize material from the meteoroid. The free electrons created by this ablation reflect radio waves, a fact exploited by radar aficionados.

The size of individual meteoroids detected by radar systems can be inferred by three different methods: by the radar power reflected from a Fresnel zone of the meteor trail (§ 2.2.3), by the power reflected from the meteor head (§ 2.2.4), or by the deceleration of the meteoroid as it ablates in Earth's atmosphere (also in § 2.2.4).

The first two size estimates rely on the power of the reflected radar signal. For radar micrometeors the relevant reflection is coherent. The wavelengths employed are comparable to or larger than the initial width r_0 of the ionization trail, so the radar is sensitive to the electron line density q rather than the space density. The reflected power depends on the transmitted power, the distance between the radar and the meteoroid, the mass and velocity of the meteoroid, and the (uncertain) ionization efficiency. Here we quantify this relation. A good introduction to the subject of radar meteors is given by McKinley (1961).

2.2.1. *Meteoroid Properties*

The radii of radar meteoroids range from $a \sim 3$ to ~ 40 μm. For purposes of illustration, we consider meteoroids with radius $a = 10$ μm, density $\rho = 3$ g cm^{-3}, and made of silicates such as forsterite, Mg_2SiO_4. Our default meteoroid has a mean molecular weight of 140 g mol^{-1} and a vaporization temperature of order 2000 K. We assume that the energy per bond is ~ 5 eV. This is equivalent to a heat of ablation of $\zeta \sim 2 \times 10^{11}$ ergs g^{-1}.

The mass of our default meteoroid is $m = 1.3 \times 10^{-8}$ g. The mean atomic weight is $\mu \approx 20 m_p$, where $m_p = 1.67 \times 10^{-24}$ g is the mass of a proton, while the total number of atoms in the meteoroid is $N = m/\mu \approx 4 \times 10^{14}$. The total binding energy of the meteoroid is

$$E_B \equiv \zeta m \approx 2600 \left(\frac{a}{10\ \mu{\rm m}}\right)^3 \left(\frac{5\ {\rm eV}}{\rm bond}\right) \left(\frac{\rho}{3\ {\rm g\ cm}^{-3}}\right) {\rm ergs}. \tag{6}$$

[4] The cited authors use the cumulative flux in a logarithmic mass interval, $f_{\log_{10} m} d(\log m) = f_m\, dm$. The two fluxes are related by $mf_m = f_{\log_{10} m}/\ln 10$.

A typical meteor is highly supersonic, with velocity $v \sim 40$ km s^{-1} at the top of the atmosphere, so the kinetic energy of the meteoroid is

$$\mathrm{KE} \approx 10^5 \left(\frac{a}{10\ \mu\mathrm{m}}\right)^3 \left(\frac{v}{40\ \mathrm{km\ s^{-1}}}\right)^2 \left(\frac{\rho}{3\ \mathrm{g\ cm^{-3}}}\right) \mathrm{ergs}, \quad (7)$$

much larger than the binding energy.

2.2.2. *The Ionization Trail*

As the meteoroid passes through the atmosphere, it collides with air molecules and is ablated. Because the kinetic energy per meteoroid atom is in excess of 100 eV, while the ionization potential is of order 10 eV (depending on the atomic species), collisions between ablated atoms and air molecules may ionize either or both particles. The number of ions produced by each meteoroid atom is denoted by β in the meteor literature. It is electrons from these ionized atoms that reflect the radar signal.

If the mass-loss rate of a meteoroid traveling at velocity v is dm/dt, the number of ions produced per centimeter along the flight path is

$$q = -\frac{\beta}{\mu v}\frac{dm}{dt}. \quad (8)$$

The rate at which the meteoroid ablates depends on the ambient air density, which increases exponentially as the meteoroid descends through the atmosphere. In other words, the mass-loss rate increases rapidly with time. The pressure scale height H_p of the atmosphere is roughly constant, since $H_p = kT/(\mu_{\mathrm{air}} g)$ and the air temperature $T \approx 200$ K. The line density q reaches a maximum just before the meteoroid vanishes, with most of the matter being deposited in the last scale height of its path. Taking $-v\,dt = H_p$, we find

$$q = \frac{3}{2}\frac{\beta m}{\mu H_p}, \quad (9)$$

where the factor of 3/2 comes from the more accurate calculation outlined in the Appendix.

The value of β depends strongly on velocity v, but the range of v for typical extrasolar meteors at Arecibo or AMOR is 20–60 km s^{-1}, with most near 40 km s^{-1}. Jones (1997) and Jones & Halliday (2001) examine β using a combination of laboratory experiments and observational data. For iron atoms they find $\beta \approx 0.6(v/40\ \mathrm{km\ s^{-1}})^{3.12}$ (with $v < 60$ km s^{-1}). For more realistic compositions they expect β to be a factor of 5 smaller. For a meteoroid with mean atomic weight $\mu = 20 m_p$ (as for forsterite),

$$q \approx 6\times 10^7 \left(\frac{\beta}{0.1}\right)\left(\frac{a}{10\ \mu\mathrm{m}}\right)^3 \left(\frac{\rho}{3\ \mathrm{g\ cm^{-3}}}\right)\left(\frac{6\ \mathrm{km}}{H_p}\right) \mathrm{cm^{-1}}. \quad (10)$$

The height at which the meteoroid ablates can be estimated by finding the height at which the binding energy of the meteoroid decreases most rapidly. The rate of change of the binding energy is

$$\zeta \frac{dm}{dt} = -\Lambda \pi a^2 \frac{1}{2}\rho_a v^3, \quad (11)$$

where ρ_a is the mass density of the atmosphere at the height of the meteoroid and Λ is the fraction of the kinetic energy flux that goes toward ablating the meteoroid. Taking the derivative of this expression with respect to time and setting the result equal to zero yields the relation

$$-\frac{2}{3m}\frac{dm}{dt} = \frac{1}{\rho_a}\frac{d\rho_a}{dt} + \frac{3}{v}\frac{dv}{dt}. \quad (12)$$

We show in the Appendix that the last term is typically smaller than either of the other two, or at best comparable, so we ignore it. Using equation (11) and setting $d\rho_a/dt = \rho_a v/H_p$, we find that the meteoroid ablates when the atmospheric density is

$$\rho_a^* = \rho \frac{4}{\Lambda}\left(\frac{a}{H_p}\right)\left(\frac{\zeta}{v^2}\right). \quad (13)$$

Using typical values, we find

$$\rho_a^* \approx 2.6\times 10^{-9}\left(\frac{\rho}{3\ \mathrm{g\ cm^{-3}}}\right)\left(\frac{10^{-1}}{\Lambda}\right)\left(\frac{a}{10\ \mu\mathrm{m}}\right) \times \left(\frac{\zeta}{2\times 10^{11}\ \mathrm{cm^2\ s^{-2}}}\right)\left(\frac{40\ \mathrm{km\ s^{-1}}}{v}\right)^2\left(\frac{6\ \mathrm{km}}{H_p}\right). \quad (14)$$

Using an MSIS model atmosphere,[5] we find that this density occurs at a height of 92 km, comparable to the observed height at both AMOR and Arecibo.

On the other hand, radar data from Jodrell Bank and from Ottawa show that radar meteoroids detected by those systems also ablate at heights near 95 km (McKinley 1961), despite the fact that they have line densities $q \approx 10^{14}$ cm^{-1}, 6 orders of magnitude larger than the Arecibo or AMOR meteoroids traveling at the same velocity. These larger meteoroids are still much smaller than the mean free path, so that aerodynamic effects seem unlikely to explain the difference; nevertheless, something must differ between the two classes of objects, or else the more massive Jodrell Bank meteoroids would be ablated 5 scale heights below the less massive meteoroids discussed here. One possibility that has been suggested is that the more massive meteoroids (those seen at Jodrell Bank and Ottawa) fragment into smaller pieces, which are then rapidly ablated. The observed heights of the Arecibo and AMOR events suggest that for micrometeoroids that do not fragment $\Lambda \approx 0.1$ and $\zeta \approx 10^{11}$ cm^2 s^{-2}.

We stated above that the initial width r_0 of the ionization trail was comparable to or smaller than the radar wavelength. We estimate r_0 as follows. The cross section of an atom is roughly $\sigma = \pi d^2$, with $d \approx 2\times 10^{-8}$ cm; at 95 km the MSIS atmosphere has $T = 171$ K and a mean free path of $l \approx 37$ cm. However, the typical meteoroid atom has an atomic mass about twice that of a nitrogen atom. In a collision between a meteoroid atom and a nitrogen molecule, the momentum will not be shared equally between the two N atoms; the binding energy of the N_2 is much less than the kinetic energy of the meteoroid atom. Neglecting the momentum carried away by the slower of the two rebounding N atoms, we find that the final velocity of the meteoroid atom is about $\frac{2}{3}$ of its initial velocity for a head-on collision. After n such collisions, the velocity is $v_n = (\frac{2}{3})^n v_0$. Setting v_n equal to twice the thermal velocity at 95 km, we find that the meteoroid atom is

[5] Available at http://nssdc.gsfc.nasa.gov/space/model/models/msis.html.

TABLE 1
RADAR PARAMETERS

Parameter	Arecibo	AMOR
P_T (kW)	2000	100
P_n (ergs s^{-1})	10^{-8}	1.6×10^{-7}
G_T	10^6	430
G_R	10^6	130
R_0 (km)	100	230
λ (cm)	70	1145
Beam dimensions (deg)	$1/6 \times 1/6$	3×18
A_G (km^2)	0.9	50
$A_{\rm col}$ (km^2)	10^{-2}	8
Meteor Properties		
$q_{\rm min}$ (cm^{-1})	10^7	7×10^8
$m_{\rm min}$ (g)	3×10^{-9}	2×10^{-7}
$a_{\rm min}$ (μm)	6	25

thermalized after $n \sim 10$ collisions. Thus, $r_0 \approx n^{1/2} l$, or about 100 cm. A strict lower limit to the thermalization time is $\tau_{\rm th} = l/v$, about 10 μs, much shorter than the time between radar pulses. Using different arguments, Manning (1958) and Bronshten (1983) obtain similar results. After this initial rapid diffusion, ordinary thermal diffusion sets in and the trail radius slowly increases.

The initial electron density is

$$n_e = \frac{q}{\pi r_0^2} \approx \left(2 \times 10^3 \text{ cm}^{-3}\right)\left(\frac{\beta}{0.1}\right)\left(\frac{a}{10\ \mu\text{m}}\right)^3 \times \left(\frac{6 \text{ km}}{H_p}\right)\left(\frac{\rho}{3 \text{ g cm}^{-3}}\right) \text{cm}^{-3}. \quad (15)$$

The plasma frequency $\nu_p \approx 0.39$ MHz is well below the frequency employed in the radar systems, so the radar beam will penetrate through the trail, ensuring that all the electrons will reflect. The average distance between electrons is $n^{-1/3} \approx 0.1$ cm, much less than the wavelength of either AMOR or Arecibo, so the reflected emission will be coherent in both systems.

The thermal diffusion mentioned above eventually causes the trail radius to exceed the wavelength of the radar. This diminishes the visibility of the trail, particularly for trails formed at great heights, or for short-wavelength radar. A recent discussion of this "height ceiling" can be found in Campbell-Brown & Jones (2003).

2.2.3. *Minimum Detectable Meteoroid Size at AMOR*

We proceed to calculate the power collected by the radar receiver at AMOR. The relevant properties of the AMOR radar (as well as those for the Arecibo setup) are listed in Table 1. An electron a distance R from the radar sees a flux $P_T G_T/4\pi R^2$, assuming that the radar transmits a power P_T and has an antenna gain G_T. The gain is defined as 4π sr (the solid angle into which an isotropic emitter radiates) divided by the solid angle of the radar beam; the latter is roughly $(\lambda/D)^2$, where D is the radius or length of the antenna. Hence, the effective area of the antenna is related to the gain by $A_{\rm eff} = G_T \lambda^2/4\pi$. The electron scatters the incident wave, emitting a power $(3/2)P_T G_T \sigma_{\rm T}/4\pi R^2$ back toward the radar; the factor 3/2 arises because Thomson scattering is that of a Hertzian dipole rather than isotropic. The receiving antenna (which in the case of Arecibo is the same as the transmitting antenna) captures a fraction $A_{\rm eff}/4\pi R^2$ of this scattered power. The power received at the antenna from a single electron is

$$\Delta P_e = P_T\left(\frac{3 G_T G_R}{128\pi^3}\right)\left(\frac{\sigma_{\rm T}\lambda^2}{R^4}\right). \quad (16)$$

We have allowed for the possibility that the gains for the receiver and transmitter are different, as is indeed the case at AMOR.

The amplitude of the electric field at the receiver is

$$\Delta A_e = \sqrt{2r\Delta P_e}, \quad (17)$$

where r is the impedance of the receiver.

The instantaneous signal amplitude received from a meteor trail is found by summing over all the electrons along the track:

$$A(t) = \int_{s_1}^{s_2} (2r\Delta P_e)^{1/2} q(s) \sin(\omega t - 2kR)\, ds, \quad (18)$$

where ω is the angular frequency of the radar and $k = 2\pi/\lambda$. The total distance from the radar to the trail and back is $2R$, whence the factor 2 in the argument of the sine. We measure s along the trail starting from the point X on the trail at which q reaches its maximum. The distance between the radar and point X is denoted by R_0, while the angle between the line of sight and the meteor trail at X is denoted by $\pi/2 + \theta$.

Near X,

$$R \approx R_0\left[1 + \frac{s}{R_0}\theta + \frac{1}{2}\left(\frac{s}{R_0}\right)^2\right], \quad (19)$$

where we assume $\theta \ll 1$. Define $\chi = \omega t - 2kR_0$ and $z = 2s/(R_0\lambda)^{1/2}$. Then

$$A(t) = \sqrt{2r\Delta P_e}\, q\, \frac{\sqrt{R_0\lambda}}{2} \times \int_{z_1}^{z_2} \sin\left(\chi - 2\pi\sqrt{\frac{R_0}{\lambda}}\theta z - \frac{\pi z^2}{2}\right) dz. \quad (20)$$

When $\theta \ll (\lambda/R_0)^{1/2}$, the integral reduces to a Fresnel integral, which is an oscillating quantity of order unity. The peak power at AMOR is then

$$P_R \approx P_T \frac{3G_T G_R}{256\pi^3}\left(\frac{\lambda}{R_0}\right)^3 q^2 \sigma_{\rm T}. \quad (21)$$

When $\theta \gtrsim (\lambda/R_0)^{1/2}$, the integral cuts off at $z \lesssim \frac{1}{4}$. In other words, the AMOR detector is sensitive only to micrometeor trails within an angle $\theta \approx (\lambda/R_0)^{1/2}$ of the perpendicular to the line of sight.

The minimum detectable line density for AMOR is

$$q_{\rm min} = \frac{1}{\sqrt{\sigma_{\rm T}}}\left(\frac{P_R}{P_T}\right)^{1/2}\left(\frac{256\pi^3}{3G_T G_R}\right)\left(\frac{R_0}{\lambda}\right)^{3/2}. \quad (22)$$

The minimum detectable power at AMOR is $P_n = 1.6 \times 10^{-13}$ W, the transmitted power is $P_T = 100$ kW, while the gains are $G_T = 430$ and $G_R = 130$. The typical range is $R_0 \approx 200$ km, leading to

$$q_{\rm min} \approx 7 \times 10^8 \ {\rm cm}^{-1}. \quad (23)$$

Using equation (9), the minimum detectable mass is

$$m_{\rm min} \approx 2 \times 10^{-7} \ {\rm g}, \quad (24)$$

corresponding to a minimum radius of

$$a_{\rm min} \approx 25\left(\frac{3 \ {\rm g \ cm^{-3}}}{\rho}\right)^{1/3}\left(\frac{0.1}{\beta}\right)^{1/3}\left(\frac{R_0}{200 \ {\rm km}}\right)^{2/3} \mu{\rm m}. \quad (25)$$

We are now in a position to estimate the collecting area $A_{\rm col}$ of the AMOR detector (as a meteor detector, not as a radar). The collecting area is the product of the sensitivity-weighted geometric area A_G imaged by the radar and the fraction of solid angle $(\lambda/R_0)^{1/2}$ to which it is sensitive:

$$A_{\rm col} \approx \sqrt{\frac{\lambda}{R_0}} A_G. \quad (26)$$

We define the sensitivity-weighted geometric area as

$$A_G \equiv \int \frac{F(m)}{F(m(R_{\rm min}))} R \, dR \, d\phi. \quad (27)$$

Here $F(m)$ is the flux of particles of the minimum detectable mass $m = m_{\rm min}(R)$; the latter is a function of R, the distance between the radar and the meteor trail. We assume that $m_{\rm min} \propto q_{\rm min} \propto R^{3/2}$, where the last scaling comes from equation (22), and that $F(m) \propto m^{-1}$ as an analytically simpler version of equation (5). With these assumptions,

$$A_G \approx 2R_{\rm min}^2 \Delta\phi\left(\sqrt{\frac{R_{\rm max}}{R_{\rm min}}} - 1\right). \quad (28)$$

The AMOR beam has a width of $\Delta\phi \approx 3^\circ$ and extends from 12° to 30° above the horizon. We further assume that all the meteors are detected at heights of $\sim$90 km. This implies that the lower and upper limits to the integration are $R_{\rm min} = 165$ km and $R_{\rm max} = 430$ km. We find $A_G \approx 10^{13}$ cm^2. The collecting area of the radar system is then

$$A_{\rm col} \approx 8 \ {\rm km}^2. \quad (29)$$

From Figure 1*b* in Baggaley (2000), we estimate that in 4 yr of continuous operation AMOR detected $\sim 10^4$ extrasolar meteors, so we estimate the flux as

$$mf_m\left(m = 2 \times 10^{-7} \ {\rm g}\right) \approx 4 \times 10^{-16} \ {\rm cm^{-2} \ s^{-1}}. \quad (30)$$

From the same paper, we estimate the number of extrasolar meteors detected from Baggaley's "point source" to be about 200, leading to a flux 50 times smaller. Both fluxes are plotted in Figure 1, along with flux estimates from *Ulysses*, *Galileo*, and Arecibo.

Figure 2 shows the same data as a differential mass flux. In this plot the bulk of the mass flux is represented by the highest point, making it easy to see that most of the mass of interstellar meteoroids reaching the inner solar system comes in the form of $\sim$0.3 μm objects. On the same figure we have plotted the size distribution found by Kim & Martin (1995), normalized to a hydrogen number density of 0.1 and assuming that half the metals are in the form of dust grains.

2.2.4. *Minimum Detectable Meteoroid Size at Arecibo*

The minimum detectable meteoroid size for Arecibo can be calculated in a similar manner, starting from equations (16)

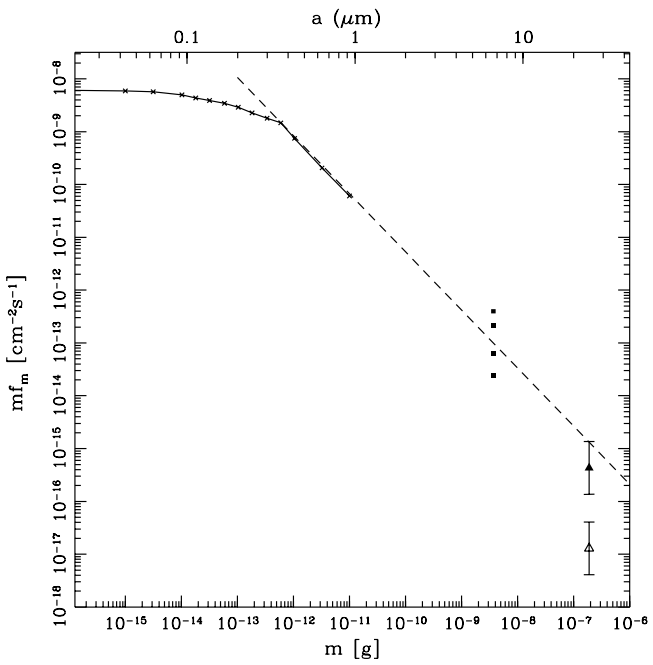

FIG. 1.—Measured cumulative fluxes of extrasolar particles. The data are from the *Ulysses* and *Galileo* satellites (*crosses joined by solid line*), the Arecibo radar (*filled squares*), and the AMOR radar (*filled triangle*). The open triangle represents the "point source" seen by the AMOR radar. The dashed line represents the $mf_m \propto m^{-1.1}$ scaling first noted by Landgraf et al. (2000) and given in eq. (5). The upper axis gives the particle radius a in microns, assuming that the meteoroids have a density of 3 g cm^{-3}.

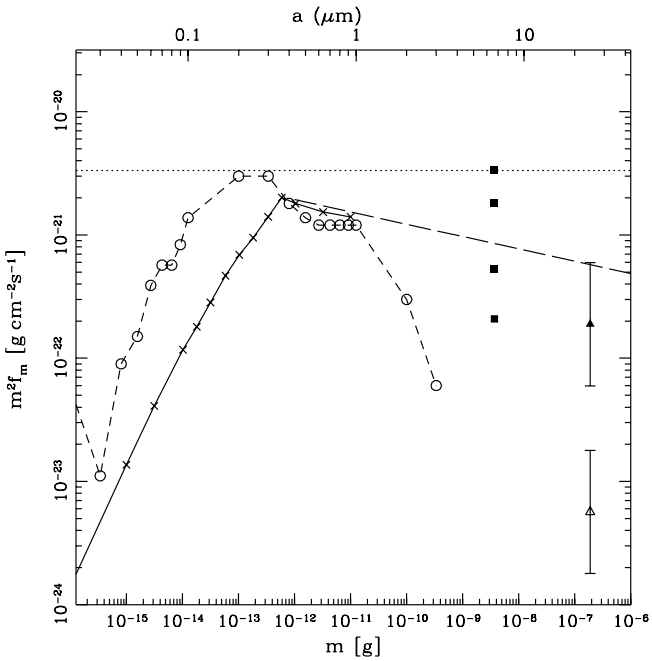

FIG. 2.—Measured differential mass fluxes, $m \times mf_m$, with units of g cm^{-2} s^{-1}, of extrasolar micrometeoroids. The long-dashed line is the Landgraf et al. (2000) scaling, while the dotted line is the limit found by assuming that half of all the metals in the local ISM (with $n = 0.1$ cm^{-3}) are in the form of grains. The filled squares are the fluxes reported by the Arecibo radar. The filled triangle is the flux estimated from the spatially distributed flux in Fig. 2 of Baggaley (2000). The open triangle is the flux in Baggaley's "point source." The horizontal dotted line is the upper limit on the flux given by assuming that half of all the heavy elements are in dust grains. The dashed line joining open circles is the flux corresponding to the ISM dust size distribution found by Kim & Martin (1995), normalized to the dotted line. This figure suggests that the bulk of the mass in dust consists of particles with masses of order 10^{-13} g, or sizes of order two-tenths of a micron.

and (17). Arecibo uses a much shorter wavelength than AMOR, 70 cm rather than 1145 cm. Arecibo also has a much narrower beam than AMOR, $\sim$500 m versus $\sim$10 km. It is thus insensitive to trails traveling across the beam, in contrast to AMOR. Since trails observed perpendicular to the line of sight have long coherence lengths, AMOR is sensitive to fairly small meteoroids despite the rather modest power and antenna gains employed. Arecibo, by contrast, is sensitive primarily to vertical trails, which have short coherence lengths (a quarter of a wavelength, less than 20 cm). This is compensated for by the much larger gains and by the larger transmitted power of the Arecibo radar.

The short wavelength employed makes the Arecibo radar sensitive to diffusion of electrons across the meteoroid trail. The Arecibo radar beam is roughly vertical, with a half opening angle of $\frac{1}{6}$ deg, so at a height of 100 km it is about 500 m wide. Typical Arecibo meteor trails are a few kilometers long, so they are within a tenth of a radian or so of the vertical. Thus, the ion trail left by an Arecibo meteoroid diffuses primarily horizontally, since the density along the trail varies on kilometer scales. As shown above, the initial trail width is of order 100 cm, but this width increases over time as a result of diffusion. The diffusion coefficient $D \sim c_s l \sim 3 \times 10^5$ cm^2 s^{-1}, where $c_s \approx 3 \times 10^4$ cm s^{-1} is the sound speed and $l \approx 10$ cm is the mean free path of air molecules. In the horizontal direction the Fresnel length is $L_F \equiv (R_0 \lambda)^{1/2} \approx 3 \times 10^4$ cm, much larger than the initial beamwidth $r_0 \approx 100$ cm. The time to diffuse horizontally over a Fresnel zone is $L_F^2/D \approx 3000$ s, so diffusion is irrelevant for a vertical trail. However, for a trail 0.1 rad off the vertical, the time to diffuse $\lambda/4$ in the vertical direction is about 13 ms. This will limit the time the beam remains visible to the radar at a given height to about 13 ms for a typical meteor. This is consistent with the trail lengths observed by Mathews et al. (1997).

We have already noted that the meteor trail is much narrower than the Fresnel length of the Arecibo radar; then all the electrons in a patch of length of order $\lambda/2$ along the trail radiate coherently. Suppose that $N_{\rm ch}$ is the number of coherently emitting electrons in such a patch. The amplitude of the electric field at the receiver from a single patch is

$$A \approx \sqrt{2r\Delta P_e} N_{\rm ch}. \tag{31}$$

The vertical resolution of the Arecibo antenna is $L \approx 150$ m, so that there are $N_p \sim L/\lambda \approx 200$ patches radiating in a resolution length. The signal observed at Arecibo varies on a length scale much shorter than the atmospheric scale height, indicating that the mass-loss rate fluctuates rapidly. We assume that these fluctuations occur on scales smaller than L, so that the electric field from each patch adds incoherently. The power received by the detector is

$$P_{\rm Arecibo} = P_T \left(\frac{3 G_T G_R}{128 \pi^3}\right) \sqrt{\frac{L}{\lambda}} \left(\frac{\sigma_{\rm T} \lambda^2}{R_0^4}\right) N_{\rm ch}^2. \tag{32}$$

Since the coherence length along the (assumed vertical) trail is of order λ, the number of coherently scattering electrons is simply related to the line density,

$$N_{\rm ch} \approx q \frac{\lambda}{2}. \tag{33}$$

The expression for the power becomes

$$P = P_T \left(\frac{3 G_T G_R}{512 \pi^3}\right) \sqrt{\frac{L}{\lambda}} \left(\frac{\lambda}{R_0}\right)^4 q^2 \sigma_{\rm T}. \tag{34}$$

For a given transmitted power, wavelength, and antenna gain, this is smaller than the equivalent expression given by equation (21) by the ratio

$$\frac{\sqrt{\lambda L}}{R_0} \approx 10^{-4}, \tag{35}$$

using values for Arecibo. Worse, the power scales as λ^3 (or as $\lambda^{3.5}$ for Arecibo), so the $\sim$15 times shorter wavelength employed by Arecibo reduces the received power by another factor of $\sim$3000. However, these two factors are more than compensated for by the much larger gains of the Arecibo antenna. The net effect is that despite its higher power and much larger gain, the Arecibo radar can detect meteoroids that are a factor of 7–10 smaller in radius than the AMOR setup, but no smaller.

Define the signal-to-noise ratio $S/N \equiv P/P_n$, where P_n is the noise power for the Arecibo receiver. Using this definition and solving for q,

$$q = \frac{1}{\sqrt{\sigma_T}} \left(\frac{P_n}{P_T}\right)^{1/2} \left(\frac{512\pi^3}{3G_T G_R}\right)^{1/2} \left(\frac{\lambda}{L}\right)^{1/4} \left(\frac{R_0}{\lambda}\right)^2 (\mathrm{S/N})^{1/2}. \quad (36)$$

Using the values in Table 1, we find $q \approx 10^7$ cm^{-1}. Using equation (9), we find

$$m \approx 3 \times 10^{-9} \left(\frac{0.1}{\beta}\right) \left(\frac{R_0}{100 \text{ km}}\right)^2 \left(\frac{150 \text{ m}}{L}\right)^{1/4} (\mathrm{S/N})^{1/2} g. \quad (37)$$

The corresponding meteoroid radius is

$$a \approx 6 \left(\frac{3 \text{ g cm}^{-3}}{\rho}\right)^{1/3} \left(\frac{0.1}{\beta}\right)^{1/3} \left(\frac{R_0}{100 \text{ km}}\right)^{2/3} \times \left(\frac{150 \text{ m}}{L}\right)^{1/12} (\mathrm{S/N})^{1/6} \ \mu\text{m}. \quad (38)$$

A firm lower limit for the size of the meteoroids seen at Arecibo is found by noting that the energy per meteoroid atom is $\sim$100 eV. Since the ionization potential of either atoms or molecules is typically of order 10 eV, a single meteoroid atom can free at most 10 electrons. Taking $\rho = 3$ g cm^{-3} and $\beta = 10$, we find $a_{\min} \approx 1.3$ μm.

From equation (34) and noting that $G_R \lambda^2 = \text{const}$, we see that, as long as λ is larger than the initial radius r_0 of the trail, $P \propto \lambda^{1.5}$. Some Arecibo meteors are seen at both 430 and 50 MHz (D. D. Meisel 2003, private communication). This suggests that the volume occupied by the reflecting electrons has linear dimensions smaller than $\lambda/2 \approx 35$ cm.

For example, it might be thought that the meteoroid itself captures enough electrons to scatter the radar beam. However, this is not possible. The number of charges required to reflect the beam is given by equation (32), except that in this case there is only one emitting region (the meteor) so the factor $(L/\lambda)^{1/2}$ should be dropped. We find $N_{\mathrm{ch}} \approx 10^9$; the meteoroid is charged to a (negative) voltage of $V = 4.8 \times 10^5 (3\ \mu\text{m}/a)$ V. Charging the meteoroid to such a high voltage leads to rapid electron emission by quantum tunneling, also known as field emission (Fowler & Nordheim 1928). The discharge current (in statamp cm^{-2}) is given by

$$I = \frac{e}{2\pi h} \frac{(\mu/\phi)^{1/2}}{\phi + \mu} (eE)^2 \exp\left(-\sqrt{\frac{8\pi^2 m_e}{h^2}} \frac{4\phi^{3/2}}{3eE}\right), \quad (39)$$

where $E \approx V/a$ is the electric field near the surface of the meteor, ϕ is the work function, and μ is the Fermi energy. Both of the latter have values of order 5 eV.

We make the optimistic assumption that the meteoroid gains an electron for every atom it collides with in the atmosphere, $I_{\mathrm{in}} = e n_a^* v$, also in statamp cm^{-2} (n_a^* is the number density of air molecules at the height where the meteoroid ablates; see eq. [14]). Setting these two currents equal, we find the equilibrium field $E \approx 3.6 \times 10^7$ V cm^{-1} or a maximum voltage of $V = 10^4 (a/3\ \mu\text{m})$. The number of charges on the meteoroid cannot exceed $N_{\mathrm{ch,\,max}} \approx 2 \times 10^7 (a/3\ \mu\text{m})^2$, a factor of 30 too small to explain the Arecibo observations. The meteor head signal must be due to electrons in the atmosphere around or trailing the meteor.

One can also estimate a dynamically, if one can measure the rate of deceleration of the meteoroid due to atmospheric drag:

$$m \frac{dv}{dt} = -\Gamma \rho_a v^2 A_m, \quad (40)$$

where Γ is the drag coefficient and A_m is the area of the meteoroid. The radar measures dv/dt, v, and the height of the meteor. Using a standard atmospheric model, the density ρ_a can be determined. For micrometeoroids, which have a size less than the mean free path for collisions, $\Gamma = 1$, so the ratio m/A_m can be determined directly from measured quantities. Janches et al. (2000) refer to this ratio as the ballistic parameter, BP. We assume spherical meteoroids, so BP $\approx 4\rho a/3$. Then a simple estimate for a is

$$a = \frac{3}{4} \frac{\mathrm{BP}}{\rho}. \quad (41)$$

Janches et al. (2000) find a range of ballistic parameters, ranging down to 10^{-3} g cm^{-2} or slightly lower, leading to

$$a_{\min} \approx 2.5 \left(\frac{3 \text{ g cm}^{-3}}{\rho}\right) \left(\frac{\mathrm{BP}}{10^{-3} \text{ g cm}^{-2}}\right) \ \mu\text{m}. \quad (42)$$

This is a factor of 2 smaller than the radius estimate based on received radar power, or a factor of 8 smaller when considering the meteor mass. For the meteors with the smallest BP, the size drops to 1 μm or less. It is very difficult to see how the power reflected from such a low-mass meteoroid could be detected at Arecibo, suggesting that the micrometeoroids have a density closer to 1 g cm^{-3} than to 3 g cm^{-3}. In fact, if we set $\rho = 1$ g cm^{-3}, we find $a \sim 8.5$ and $\sim$7.5 μm from the power and BP estimates, respectively.

The fluxes observed at Arecibo are given by Meisel, Janches, & Mathews (2002b); they are also shown in Figure 1.

3. PROPAGATION OF LARGE GRAINS THROUGH THE ISM

We have seen that AMOR can only detect grains with masses $\gtrsim 2 \times 10^{-7}$ g, corresponding to a grain radius $a \approx 25$ μm for silicate dust (mass density $\rho \approx 3.5$ g cm^{-3}). Similarly, Arecibo can detect particles with $a \gtrsim 6$ μm. Thus, we restrict our attention to "large" (by interstellar dust standards) grains, with $a \gtrsim 10$ μm.

For such large grains in the interstellar medium (ISM), radiation pressure can be ignored. The force due to radiation pressure is $F_{\mathrm{rad}} = \pi a^2 \langle Q_{\mathrm{pr}} \rangle \Delta u_{\mathrm{rad}}$, where $\langle Q_{\mathrm{pr}} \rangle$ is the radiation pressure efficiency factor averaged over the interstellar radiation field (ISRF) and Δu_{rad} is the energy density in the anisotropic component of the ISRF. Adopting the ISRF for the solar neighborhood (Mezger, Mathis, & Panagia 1982; Mathis, Mezger, & Panagia 1983) and a 10% anisotropy (Weingartner & Draine 2001b), $\langle Q_{\mathrm{pr}} \rangle \approx 1$ for $a \gtrsim 10$ μm and $\Delta u_{\mathrm{rad}} \approx 8.64 \times 10^{-14}$ ergs cm^{-3}. The time interval required for radiation pressure to change a silicate grain's velocity by 1 km s^{-1} (assuming that the anisotropy direction remains the same as the grain moves through space) is thus given by $\Delta t \approx (5 \times 10^8 \text{ yr})(a/10\ \mu\text{m})$. For large grains in the diffuse ISM, the forces resulting from the asymmetric

photon-stimulated ejection of electrons and adsorbed atoms are even less effective than the radiation pressure (Weingartner & Draine 2001b), so these forces can be neglected as well.

The following three influences can be significant for grains with $a \gtrsim 10$ μm: (1) the drag force, (2) grain destruction following impacts with interstellar grains or high-energy gas atoms, and (3) the magnetic force.

We consider the propagation of grains through two idealized phases of the ISM, the cold and warm neutral media (CNM and WNM, respectively). We also consider the Local Bubble (LB), i.e., the large volume of low-density, ionized gas that surrounds the Sun (see, e.g., Sfeir et al. 1999). Our adopted values for the gas temperature $T_{\rm gas}$, H number density $n_{\rm H}$, and electron fraction $x_e \equiv n_e/n_{\rm H}$ (n_e is the electron number density) in these three environments are given in Table 2. In each case we adopt the ISRF for the solar neighborhood.

The drag and magnetic forces both depend on the grain's electric charge, which is set by a balance between the accretion of electrons from the gas versus photoelectric emission and proton accretion. For large enough grains, the rates of each of these processes are proportional to the grain area; thus, the electric potential Φ of large grains is independent of the size a. Using the charging algorithm from Weingartner & Draine (2001c), we find that silicate grains with $a \gtrsim 10$ μm charge to 0.15, 0.74, and 0.94 V in the CNM, WNM, and LB, respectively.[6]

3.1. *The Drag Force*

When a grain's motion is highly supersonic, the hydrodynamic drag (i.e., the drag due to direct impacts of gas atoms and ions) does not depend on the gas temperature. In this case, the grain's speed decreases by a factor of e once it has encountered its own mass in gas. The sound speed is 0.81 km s^{-1} (6.2 km s^{-1}) in the CNM (WNM), assuming that the He number density $n_{\rm He} = 0.1 n_{\rm H}$. We expect grain speeds as low as $\sim$10 km s^{-1}, so deviations from the highly supersonic limit can be expected in the WNM. In addition to the hydrodynamic drag, there is also the Coulomb drag, which is due to long-range electric interactions between the charged grains and gas-phase ions. The Coulomb drag contributes significantly to the total drag in the WNM for drift speeds $\lesssim$10 km s^{-1}. Using the approximate drag expressions from Draine & Salpeter (1979), we find that the actual drag force (hydrodynamic plus Coulomb) in the WNM exceeds the hydrodynamic drag force calculated in the highly supersonic limit by only a factor of $\approx$2 at a drift speed of 10 km s^{-1}. For regions outside of the LB, we adopt the highly supersonic limit and assume that drag limits the distance a grain can travel to its velocity e-folding distance $D_{\rm drag}$, given by

$$D_{\rm drag} = (650\ {\rm pc}) \left(\frac{\rho}{3.5\ {\rm g\ cm^{-3}}} \right) \left(\frac{a}{10\ \mu{\rm m}} \right) \left(\frac{n_{\rm H}}{1\ {\rm cm^{-3}}} \right)^{-1}. \quad (43)$$

[6] Here and throughout this paper we take silicate optical properties from Li & Draine (2001).

TABLE 2

IDEALIZED INTERSTELLAR ENVIRONMENTS

Phase	$T_{\rm gas}$ (K)	$n_{\rm H}$ (cm^{-3})	x_e
CNM	100	30	1.5×10^{-3}
WNM	6000	0.3	0.1
LB	10^6	5×10^{-3}	1

Near the Sun, the average H density near the Galactic midplane is $n_{\rm H} \approx 1$ cm^{-3} (Whittet 1992).

In the LB, the sound speed is $\approx$100 km s^{-1}; thus, the highly subsonic limit may apply. In this case, the drag force is proportional to the grain speed. Using the Draine & Salpeter (1979) drag expressions, we find that the Coulomb drag is negligible and that

$$D_{\rm drag} = (7.8\ {\rm kpc}) \left(\frac{\rho}{3.5\ {\rm g\ cm^{-3}}} \right) \left(\frac{a}{10\ \mu{\rm m}} \right) \times \left(\frac{n_{\rm H}}{1\ {\rm cm^{-3}}} \right)^{-1} \left(\frac{T_{\rm gas}}{10^6\ {\rm K}} \right)^{-1/2} \left(\frac{v_0}{10\ {\rm km\ s^{-1}}} \right), \quad (44)$$

where v_0 is the grain's initial speed. Since the maximum extent of the LB is $\approx$250 pc (Sfeir et al. 1999) and $n_{\rm H} \approx 5 \times 10^{-3}$ cm^{-3}, drag in the LB is always insignificant, whether the subsonic or supersonic limit applies.

3.2. *The Magnetic Force*

Charged grains spiral around magnetic field lines with a gyroradius

$$r_B = (17\ {\rm pc}) \left(\frac{\rho}{3.5\ {\rm g\ cm^{-3}}} \right) \left(\frac{\Phi}{0.5\ {\rm V}} \right)^{-1} \times \left(\frac{B}{5\ \mu{\rm G}} \right)^{-1} \left(\frac{v}{10\ {\rm km\ s^{-1}}} \right) \left(\frac{a}{10\ \mu{\rm m}} \right)^2. \quad (45)$$

Although the magnetic field strength B has not been measured in the LB, $B \sim 5$ μG just outside the LB, with the random component dominating the ordered component (Heiles 1998). Thus, the magnetic force can significantly deflect grains with $a \approx 10$ μm. Since $r_B \propto a^2$, the importance of the magnetic deflection rapidly decreases with grain size.

3.3. *Grain Destruction*

When a grain travels through the ISM, it is subjected to various agents of destruction, including:

1. Sputtering, in which gas-phase ions strike the grain and remove grain surface atoms, which then enter the gas. It is useful to distinguish between thermal sputtering (due to thermal motion of the gas atoms) and nonthermal sputtering (due to the motion of the grain with respect to the gas).
2. Shattering and vaporization in grain-grain collisions.
3. For ices, sublimation and photodesorption.

Thermal and nonthermal sputtering have been extensively discussed by Tielens et al. (1994). Applying their analysis, we find that sputtering of grains with $a \gtrsim 10$ μm can be neglected in all environments of interest.

The physics of grain-grain collisions has been treated extensively by Tielens et al. (1994) and Jones, Tielens, & Hollenbach (1996). When the relative speed exceeds $\approx$3 km s^{-1} (see Table 1 in Jones et al. 1996), a crater forms on the larger grain (the target). A portion of the evacuated mass remains on the grain as a crater lip. The rest of the crater mass is removed, both as vapor and as shattering fragments. The shattering fragments dominate the vapor, and the largest fragment is typically somewhat larger than the smaller impacting grain (the projectile). When the relative speed exceeds $\sim$100 km s^{-1} (depending on the target and projectile materials; see Table 1 in Jones et al. 1996), the larger grain is

entirely disrupted, and the largest shattering fragment can be a substantial fraction of the target size. For our purposes, the cratering regime is generally applicable.

Jones et al. (1996) give simple approximations for the (material-dependent) ratio of the crater mass (M_c) to the projectile mass ($M_{\rm proj}$). Interstellar dust is thought to be dominated by two populations: silicates and carbonaceous (e.g., graphite) grains. For a head-on collision between a silicate target and either a silicate or graphite projectile, the Jones et al. (1996) results can be approximated by

$$\frac{M_c}{M_{\rm proj}} \approx 18\left(\frac{v}{10\ {\rm km\ s^{-1}}}\right) + 29\left(\frac{v}{10\ {\rm km\ s^{-1}}}\right)^2, \quad (46)$$

where v is the grain-grain relative speed. This empirical approximation reproduces detailed calculations, using equation (1) and Table 1 from Jones et al. (1996), to within 10% when 5 km s^{-1} $\leq v \leq$ 100 km s^{-1}.

The crater mass is approximately 4.2 (2.2) times bigger for a graphite (ice) target. We assume that equation (46) applies to all collisions and that the entire crater mass is ejected. This is a conservative assumption, since the crater mass should actually be smaller for oblique collisions, and a portion of the crater mass will form a lip. On the other hand, we underestimate destruction if target grains are made of less resilient material than silicate or if the grains are fluffy.

Since the mass in dust is $\approx$0.011 times the mass in H (in all gas-phase forms) in the ISM (see, e.g., Weingartner & Draine 2001a), the distance a grain can travel before it loses half its mass is given by

$$D_{\rm dest} \approx (40.2\ {\rm kpc})\left(\frac{\rho}{3.5\ {\rm g\ cm^{-3}}}\right)\left(\frac{a}{10\ \mu{\rm m}}\right)\left(\frac{n_{\rm H}}{1\ {\rm cm^{-3}}}\right)^{-1} \times \left[18\left(\frac{v}{10\ {\rm km\ s^{-1}}}\right) + 29\left(\frac{v}{10\ {\rm km\ s^{-1}}}\right)^2\right]^{-1}, \quad (47)$$

yielding $D_{\rm dest} \approx 860$ pc for $v = 10$ km s^{-1} (and with other canonical parameter values as in eq. [47]).

3.4. *The Survival Probability*

In Figure 3 we plot $D_{\rm drag}$, r_B, and $D_{\rm dest}$ versus v for four grain sizes, covering the range of interest. Because of the expected dramatic decrease in flux with a (see, e.g., eq. [92]), we are not interested in $a \gtrsim 100$ μm. We adopt $\rho = 3.5$ g cm^{-3}, $n_{\rm H} = 1$ cm^{-3}, $\Phi = 0.5$ V, and $B = 5$ μG and assume supersonic grain speeds for these plots. For all of the considered grain sizes, magnetic deflection dominates the other two processes when $v = 10$ km s^{-1}, while destruction dominates when v is greater than a few to several times 10 km s^{-1}. The drag force is never dominant. The detailed analysis of the dynamics of a charged grain in a region with both ordered and random magnetic field components is beyond the scope of this paper. Thus, we simply assume that

$$f_{\rm survive} = \begin{cases} 1, & d < \min(r_B, D_{\rm dest}), \\ 0, & d > \min(r_B, D_{\rm dest}). \end{cases} \quad (48)$$

The grain velocity used in evaluating r_B and $D_{\rm dest}$ should be taken with respect to the ambient ISM. However, for simplicity, we use the velocity with respect to the Sun.

For LB conditions, magnetic deflection dominates destruction for grains with 10 μm $< a <$ 100 μm when $v <$ 100 km s^{-1}. For example, for $a = 10$ μm, $D_{\rm dest} = r_B$ when $v = 311$ km s^{-1} and $r_B = 281$ pc (which exceeds the maximum extent of the LB). For $a = 100$ μm, $D_{\rm dest} = r_B$ when $v = 143$ km s^{-1} and $r_B = 13$ kpc.

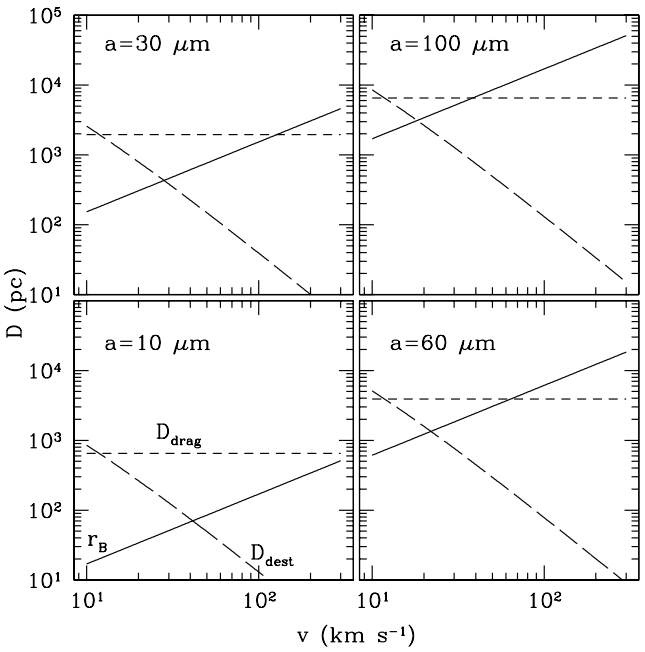

FIG. 3.—Drag distance $D_{\rm drag}$ (*short-dashed line*), gyroradius r_B (*solid line*), and grain destruction distance $D_{\rm dest}$ (*long-dashed line*) vs. grain speed v for four grain sizes, as indicated, and assuming supersonic grain speeds and $\rho =$ 3.5 g cm^{-3}, $n_{\rm H} = 1$ cm^{-3}, $U = 0.5$ V, and $B = 5$ μG.

4. DUST FROM YOUNG MAIN-SEQUENCE STARS

IRAS observations of several young main-sequence stars revealed emission at 60 and 100 μm substantially in excess of the emission from the star's photosphere (e.g., Aumann et al. 1984; Gillett 1986). This "Vega phenomenon" (named for the first example to be observed) was attributed to circumstellar dust, which absorbs the star's optical radiation and reemits in the infrared. Shortly following this discovery, Smith & Terrile (1984) observed the optical light scattered by the dust around β Pic and found that the grains lie in an edge-on disk. More recently, disks have been imaged (in the infrared and submillimeter) around a handful of other stars (e.g., Holland et al. 1998; Schneider et al. 1999). For reviews of the Vega phenomenon and circumstellar dust disks, see Backman & Paresce (1993), Lagrange, Backman, & Artymowicz (2000), and Zuckerman (2001). It is not yet clear what fraction of Vega-like stars possess dust disks, but if these stars also possess planets, then dynamical interactions can eject the grains from the system. (Radiation pressure also removes small grains, but these are too small to be traced back to their source.)

The most massive disks, which orbit the youngest stars, have optical depths in the near-IR of order 10^{-2} to 10^{-3}. The bulk of this optical depth is contributed by grains with size $a_0 \sim \lambda/2\pi$, where λ is the wavelength, typically 1–10 μm (see below).

4.1. *Gravitational Ejection of Small Particles*

Jupiter-mass planets are seen around 5%–10% of nearby solar-type stars in radial velocity surveys. These surveys are not sensitive to planets in orbits larger than $\sim$5 AU, such as Jupiter,

so the fraction of solar-type stars with such planets is likely to be substantially higher. Observations of debris disks also hint at the presence of planets (Scholl, Roques, & Sicardy 1993; Wilner et al. 2002). This suggests that gravitational interactions between a massive planet and dust particles in debris disks are a natural means for producing interstellar meteoroids.

We estimate the ejection velocity of large (25 μm) dust grains interacting with a Jupiter-mass planet. We neglect collisions with other dust grains, an assumption that we justify at the end of the calculation, as well as radiation pressure. We follow the derivation of Öpik (1976); a good general introduction to the two-body problem can be found in Murray & Dermott (1999).

We assume that the planet, of mass M_p, orbits the star, of mass M_*, on a circular orbit of semimajor axis a_p. A test mass (the dust particle) also orbits the star. The test mass is subject to the gravity of both the planet and the star, but the planet is assumed to be immune to the gravity of the test particle. When the test particle is far from the planet, it follows a roughly Keplerian orbit around the star. When the test particle is very close to the planet, it also follows a roughly Keplerian orbit, but this time around the planet. While it is close to the planet, the test particle experiences a tidal force from the star, with a magnitude given by

$$F_* \approx \frac{GM_* m_g}{a_p^2}\frac{r}{a_p}, \tag{49}$$

where r is the distance between the test particle and the planet, G is the gravitational constant, and m_g is the mass of the dust grain. The Hill radius is the distance r at which this tidal force equals the gravitational force of the planet on the test particle, $GM_p m_g/r^2$, or

$$r_{\rm H} \equiv \left(\frac{M_p}{3M_*}\right)^{1/3} a_p, \tag{50}$$

where the factor of 3 is included for historical reasons.

We make use of the Öpik approximation; while the test body is inside the Hill sphere of the planet, we assume that the motion is described by the two-body problem in the frame revolving with the planet. This involves ignoring both the tidal force of the star and the Coriolis force associated with the motion of the planet around the star. The acceleration due to the Coriolis force is

$$a_{\rm Cor} \approx \Omega_p V, \tag{51}$$

where Ω_p is the mean motion of the planet (the angular speed of the planet's revolution about the star) and V is the velocity of the test particle in the rotating frame. A rough estimate for V is v_p, the Keplerian velocity of the planet, so the Coriolis force is larger than the tidal force by a factor $a_p/r_{\rm H} \sim \mu_p^{-1/3}$ at the Hill radius; in this section $\mu_p \equiv M_p/M_*$.

4.1.1. *Inside the Hill Sphere*

We assume that the test particle orbits the star rather than the planet. Hence, the particle follows a hyperbolic orbit relative to the planet during the close encounter. The hyperbola is specified by its eccentricity $\bar{e}$ and the transverse semimajor axis $R\bar{a}$ (note that the semimajor axis of the dust particle $\bar{a}$ should not be confused with the radius a of the dust particle). Barred elements are calculated relative to the planet. Note that $\bar{e} > 1$ and $\bar{a} < 0$. Alternately, we can specify the specific energy $\bar{E} = -GM_p/2\bar{a}$ and specific angular momentum $\bar{L} = [GM_p\bar{a}(1-\bar{e}^2)]^{1/2}$ relative to the planet. The energy is positive, so the particle would have a finite velocity as it traveled to infinity, if we ignore the effects of the star. This velocity is known as the velocity at infinity; we denote it by U.

The approximations described above allow us to find an analytic relation between the angle of deflection resulting from the encounter and the eccentricity of the (hyperbolic) orbit of the test body around the planet. We then relate the eccentricity to the periapse distance $\bar{q}$ between the planet and the test particle and the velocity at infinity.

The specific energy and angular momentum of a test mass interacting with a planet of mass M_p are given by

$$\bar{E} = \frac{1}{2}V^2 - \frac{GM_p}{\bar{r}} \tag{52}$$

and

$$\bar{L} = \bar{r}^2\frac{d\theta}{dt}. \tag{53}$$

In these expressions G is the gravitational constant, $\boldsymbol{V}$ is the velocity of the test mass relative to the planet, and $\bar{r}$ is the distance between the two bodies. The angle θ is measured from a fixed line (which we choose to be the apsidal line, which connects the test particle and the planet at the point of closest approach) and the line joining the two bodies.

The distance $\bar{r}$ is given by

$$\bar{r} = \frac{\bar{p}}{1+\bar{e}\cos\theta}. \tag{54}$$

The quantity $\bar{p} \equiv \bar{L}^2/GM_p$ is called the semilatus rectum. The periapsis distance (at closest approach) is denoted by $\bar{q}$ and is given by $\bar{q} = \bar{p}/(1+\bar{e})$.

The semilatus rectum $\bar{p}$ is related to $\bar{e}$ and $\bar{a}$ by

$$\bar{p} = \bar{a}\left(1-\bar{e}^2\right), \tag{55}$$

Note that $\bar{p} > 0$ and that $\bar{q} = \bar{a}(1-\bar{e}) > 0$. Using the definition of $\bar{a}$, we can write the specific energy in terms of $\bar{p}$ and $\bar{e}$:

$$\bar{E} = \frac{GM_p}{2\bar{p}}(\bar{e}^2 - 1). \tag{56}$$

From equation (52)

$$\bar{E} = \frac{1}{2}\bar{v}_q^2 - \frac{GM_p}{\bar{q}} = \frac{1}{2}U^2, \tag{57}$$

where $\bar{v}_q$ is the speed at closest approach and U is the speed at infinity.

From equation (54), as $r \to \infty$, the angle θ tends to

$$\theta_0 = -\arccos\frac{1}{\bar{e}}. \tag{58}$$

Referring to Figure 4 and denoting the angle of deflection by γ, simple geometry gives

$$\sin\frac{\gamma}{2} = \sin\left(\theta_0 - \frac{\pi}{2}\right) = -\cos\theta_0 = \frac{1}{\bar{e}}. \tag{59}$$

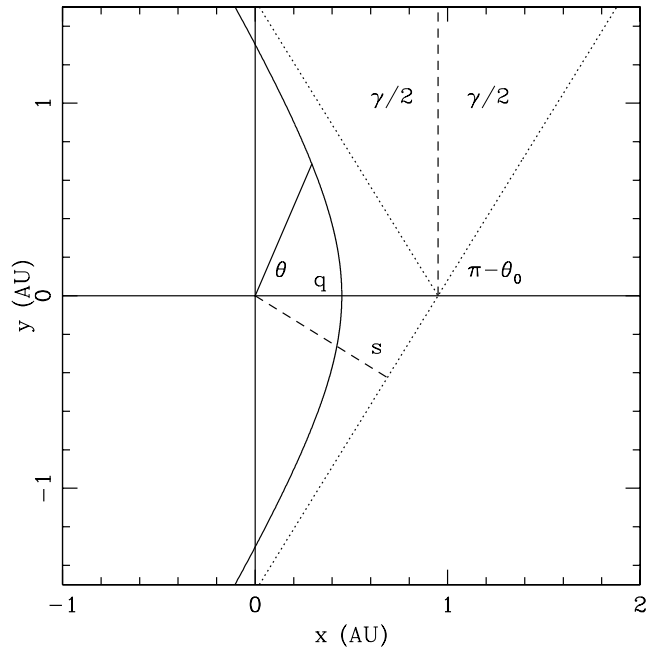

FIG. 4.—Geometry of hyperbolic motion in the two-body problem. The scattering center (the planet) is at the origin; the test particle travels along the curved line, with an initial impact parameter given by s. Its closest approach to the planet occurs as it crosses the apsidal line (chosen here to be the x-axis), when it is a distance q from the planet. The ingoing and outgoing asymptotes are denoted by dotted lines. The angle between the ingoing and outgoing asymptotes is γ.

Since $\bar{e} = 1 - (\bar{q}/\bar{a})$, we find

$$\sin\frac{\gamma}{2} = \left(1 + \frac{U^2\bar{q}}{GM_p}\right)^{-1}. \tag{60}$$

It is convenient to write this in terms of the impact parameter s. From conservation of angular momentum, $sU = \bar{q}\bar{v}_q$. We find

$$\bar{q} = \sqrt{\left(\frac{GM_p}{U^2}\right)^2 + s^2} - \frac{GM_p}{U^2}. \tag{61}$$

Using this in equation (60), we find

$$\sin\frac{\gamma}{2} = \left(1 + \frac{U^4 s^2}{G^2 M_p^2}\right)^{-1/2}. \tag{62}$$

4.1.2. *Relating U to the Orbital Elements a and e of the Test Particle*

We assume that the impact parameter s is uniformly distributed between 0 and $r_{\rm H}$. However, we still need to know U, the speed at infinity, in the frame rotating with the planet. We can find U in terms of the semimajor axis a and eccentricity e of the test particle, where the orbital elements are now calculated relative to the star. The relations between E, L, a, e, and p are as given above, but with the star playing the role of the central mass, so that M_p is replaced by M_*, the mass of the star. Since the test particle is bound to the star, $E < 0$, $a > 0$, and $e < 1$, at least until the scattering event that ejects the test particle. We restrict our attention to the case in which the planet and the test particle orbit in the same plane.

We start by resolving the particle velocity (relative to an inertial frame centered on the center of mass) into a radial v_r and a transverse v_t part. From the definition of angular momentum, the transverse velocity at the time of the close encounter is

$$v_t = \frac{L}{r} \approx v_p\sqrt{\frac{a}{a_p}\left(1 - e^2\right)}, \tag{63}$$

where $v_p = (GM_*/a_p)^{1/2}$ is the Keplerian velocity of the planet and we have made use of the fact that the star-particle distance $r \approx a_p$ (it can differ by $r_{\rm H}$) during the encounter.

The magnitude of the total velocity v is found from the expression for the energy,

$$E = \frac{1}{2}v^2 - \frac{GM_*}{a_p} = -\frac{GM_*}{2a}, \tag{64}$$

where we have again set $r = a_p$ in the first equality. Solving equations (63) and (64) for v_r,

$$v_r \approx v_p\left[2 - \frac{a_p}{a} - \frac{a}{a_p}\left(1 - e^2\right)\right]^{1/2}. \tag{65}$$

Note that if the orbits just cross, $a(1-e)/a_p = 1, 1+e = 2 - a_p/a$, and $v_r = 0$; the collision occurs at periapse. Then $U^2 = (v_t - v_p)^2 \approx v_p^2$. However, the orbit of the test particle need only pass through the Hill sphere, so that $a(1-e)/a_p \approx 1 \pm r_{\rm H}/a_p \approx 1 \pm \mu_p^{1/3}$, and the radial velocity $v_r \approx \sqrt{2}\mu_p^{1/6}v_p$, which for a Jupiter-mass planet is about $0.45v_p$. If there are multiple planets in the system, the test particle periapse need not be comparable to a_p, in which case v_r could be slightly larger than v_p. The transverse velocity v_t is always of order v_p.

To find U, we transform to the planet frame, which entails subtracting v_p from v_t:

$$U_r = v_r \approx \sqrt{2}\mu_p^{1/6}v_p, \tag{66}$$

$$U_t = v_t - v_p \approx v_p\left[\sqrt{\frac{a}{a_p}\left(1 - e^2\right)} - 1\right], \tag{67}$$

$$U^2 \approx v_p^2\left[2\mu_p^{1/3} + \left(3 - 2\sqrt{2}\right)\right]. \tag{68}$$

4.1.3. *The Change in Energy*

In the frame rotating with the planet, the close encounter simply rotates the test particle velocity by the angle γ, without changing its magnitude U. The components of the scattered velocity are

$$U_r' = U_r\cos\gamma - U_t\sin\gamma, \tag{69}$$

$$U_t' = U_r\sin\gamma + U_t\cos\gamma. \tag{70}$$

Transforming back to the inertial frame, the square of the new velocity is given by

$$\begin{aligned} v'^2 &= U_r'^2 + \left(U_t' + v_p\right)^2 \\ &= U_r^2 + U_t^2 + 2v_p(U_r\sin\gamma + U_t\cos\gamma) + v_p^2. \end{aligned} \tag{71}$$

The change in specific energy

$$\Delta E \equiv \frac{(v'^2 - v^2)}{2} \approx v_p[U_r \sin\gamma + U_t(1 - \cos\gamma)]. \quad (72)$$

The radius r does not change appreciably during the encounter. Using the relations between U and v,

$$\Delta E = v_p\left[v_r \sin\gamma + \left(v_t - v_p\right)(1 - \cos\gamma)\right]. \quad (73)$$

4.1.4. *The Small Scattering Angle Approximation*

Equation (68) shows that $U^2 \approx 0.4 v_p^2$ for test particles with $a \gg a_p$ scattering off Jupiter-mass planets. From equation (62), we find

$$\gamma \approx \frac{2GM_p}{sU^2} = 2\sqrt[3]{3}\mu_p^{2/3}\left(\frac{v_p}{U}\right)^2\left(\frac{r_{\rm H}}{s}\right). \quad (74)$$

The small-angle approximation is valid for $s \gtrsim s_\gamma$, where

$$s_\gamma \approx \mu_p\left(\frac{v_p}{U}\right)^2 a_p. \quad (75)$$

There is another constraint on the minimum value of the impact parameter s, namely, that the test particle does not physically collide with the planet. This defines $s_{\rm min}$, the impact parameter for which the periapse $\bar{q} = r_p$, where r_p is the radius of the planet. For $a \gg a_p$, $s_{\rm min} \approx r_p[\,2\mu_p(v_p/U)^2(a_p/r_p)]^{1/2}$. At 5 AU, $s_{\rm min} \approx 7r_p$ for a planet with Jupiter's mass and radius. Thus, noncollisional close encounters occur if the impact parameter satisfies

$$7r_p \lesssim s \lesssim r_{\rm H}. \quad (76)$$

For a Jupiter-mass planet at 5 AU, $s_\gamma \approx 25r_p$, about 4 times larger than the minimum impact parameter. For the same values of M_p and a_p, $r_{\rm H} \approx 750r_p$. In other words, the small-angle approximation is valid for almost any impact parameter that does not lead to a physical collision.

Assuming $\gamma \ll 1$, the change in energy due to a single close encounter for a test particle with $a \gg a_p$ is

$$\Delta E\left(\mu_p, a_p, s\right) \approx 2^{3/2}\sqrt[3]{3}\mu_p^{5/6}\left(\frac{v_p}{U}\right)^2\left(\frac{r_{\rm H}}{s}\right)v_p^2. \quad (77)$$

4.1.5. *The Ejection Velocity*

We are now in position to estimate the typical ejection velocity of a test particle interacting with a Jupiter-mass planet. The particle must have an energy satisfying $-\Delta E < E < 0$ when the last encounter occurs. On average it will emerge with an energy $E \approx \Delta E/2$ after the encounter, so it is ejected with a velocity

$$v_\infty\left(\mu_p, a_p, s\right) \approx 2\mu_p^{5/12}\left(\frac{v_p}{U}\right)\sqrt{\frac{r_{\rm H}}{s}}v_p. \quad (78)$$

Note that the ejection velocity scales as the $-\frac{1}{2}$ power of the planet's semimajor axis a_p. The scaling with the mass ratio μ_p is complicated by the appearance of the Safronov number U/v_p. From equation (68), the Safronov number is independent of μ_p for $\mu_p \ll 6 \times 10^{-4}$ but scales as $\mu_p^{1/6}$ for larger μ_p. Hence, the ejection velocity will scale as $\mu_p^{5/12}$ for Saturn-mass planets and as $\mu_p^{1/4}$ for planets significantly more massive than Jupiter. If the planet has a substantial eccentricity, as many extrasolar planets do, then $v_t \approx v_p$ and the ejection velocity will scale as $\mu_p^{1/3}$.

For a Jupiter-mass planet at 5 AU from a solar-mass star,

$$v_\infty(\mu_p, a_p, s) \approx 2\left(\frac{\mu_p}{10^{-3}}\right)^{1/3}\left(\frac{5\ {\rm AU}}{a_p}\right)^{1/2}\left(\frac{v_p}{U}\right)\sqrt{\frac{r_{\rm H}}{s}}\ {\rm km\ s^{-1}}. \quad (79)$$

Let $x = s/r_{\rm H}$; then the cross section for an encounter with impact parameter between s and $s + ds$ is $2\pi s\,ds = 2\pi r_{\rm H}^2 x\,dx$. We average over x to find the mean escape velocity. We integrate from $x_\gamma \equiv s_\gamma/r_{\rm H} \approx \mu_p^{2/3} \ll 1$ to $s = \alpha r_{\rm H}$, where α is a dimensionless constant of order unity and s_γ is the minimum value of s for which equation (74) is valid. Doing the integration,

$$\langle v_\infty \rangle = \frac{\int_{x_\gamma}^{\alpha} \pi x v_\infty(x)dx}{\int_{x_\gamma}^{\alpha} \pi x\,dx} \approx \frac{4v_\infty(r_{\rm H})}{3\sqrt{\alpha}}, \quad (80)$$

where we have neglected terms of order $\mu_p v_\infty(r_{\rm H})$; we use the notation $v_\infty(r_{\rm H}) = v_\infty(\mu_p, a_p, s = r_{\rm H})$. The rms escape velocity is calculated in a similar manner. We find

$$v_{\rm rms} \approx \sqrt{\frac{2}{\alpha}}\,v_\infty(r_{\rm H}), \quad (81)$$

so the spread in escape velocities is similar to the mean escape velocity.

For those rare encounters with $s_{\rm min} < s < s_\gamma$, the scattering angle is of order unity, and the velocity kick experienced by the particle is larger than the estimate in equation (78). We take $\sin\gamma \approx \cos\gamma \approx 1/\sqrt{2}$, so

$$\Delta E \approx v_p^2 \quad (82)$$

and

$$v_\infty \approx v_p, \quad (83)$$

much larger than the small-angle limit. About 1% of the particles will be ejected with velocities of tens of kilometers per second.

4.1.6. *Ejection Timescale Compared to Collisional Timescale*

So far we have assumed that the grains are ejected before they suffer sufficient collisions with other dust particles to alter their orbits substantially. We are now in a position to check this assumption. We start with an estimate of the dust-dust collision time. The optical depth τ for the most massive debris disks is of order 0.001. This optical depth is due to particles with radii $a \approx \lambda/2\pi$, where λ is the wavelength at which the disk is observed. Since the disks are usually detected by their IR excesses, the dust particles responsible for the optical depth have $a \approx 0.3$ μm or smaller. We are interested in larger ejected particles, with $a_{\rm eject} = 25$ μm. These larger particles will suffer collisions with a particle of size $a_{\rm target}$ after roughly $1/\tau(a_{\rm target})$ orbits, where $\tau(a_{\rm target})$ is the optical depth to particles of size $a_{\rm target}$.

Using the scaling $mf_m \propto m^{-1}$, the optical depth in particles of size $a_{\rm target}$, as viewed at a wavelength of order or smaller than $a_{\rm target}$, is

$$\tau(a_{\rm target}) = \left(\frac{0.3\ \mu{\rm m}}{a_{\rm target}}\right)\tau(a = 0.3\ \mu{\rm m}). \tag{84}$$

The typical number of orbits required for our test (ejected) particles to sweep up their own mass in smaller particles, and hence have their orbits altered substantially, or to strike a larger particle is

$$N \approx \frac{1}{\tau(a = 0.3\ \mu{\rm m})} \times \begin{cases} \left(\dfrac{a_{\rm eject}}{0.3\ \mu{\rm m}}\right)\left(\dfrac{a_{\rm eject}}{a_{\rm target}}\right)^2 & a_{\rm target} \le a_{\rm eject}, \\ \left(\dfrac{a_{\rm target}}{0.3\ \mu{\rm m}}\right) & a_{\rm target} \ge a_{\rm eject} \end{cases} \tag{85}$$

in orbital periods.

Thus, the most efficient way to alter the orbit of a particle is to collide with another particle of the same size, assuming that the mass is logarithmically distributed and that gravity plays no role in the collision. The typical number of orbits for a 25 μm size particle to collide with a particle of its own mass is $\sim 1/\tau(a = 25\ \mu{\rm m}) \approx 7 \times 10^4$.

Dust-dust collisions can also shatter the grains. The binding energy for a target grain of mass m is ζm. A collision with a grain of mass m_c moving with relative velocity v will shatter the target if the kinetic energy exceeds the binding energy of the target. Allowing for the possibility that only a fraction $f_{\rm KE}$ of the kinetic energy is available to disrupt the target, the critical mass needed to shatter the target is

$$m_c = \frac{2}{f_{\rm KE}}\frac{\zeta}{e^2 v_p^2} m. \tag{86}$$

In deriving this result we assume that the relative velocity is ev_p, corresponding to the random velocity of a grain suffering close encounters with a massive planet of semimajor axis a_p. The eccentricity of the target grain undergoes a random walk in e, starting at zero and evolving to $e = 1$, $e(t) \approx (D_e t)^{1/2}$, so we take $e = \frac{2}{3}$. The minimum mass needed to shatter the target grain is then $m_c \approx 0.5(a_p/5\ {\rm AU})m/f_{\rm KE}$, roughly a mass equal to that of the target.

How long does it take for the typical particle to be ejected? The test particles undergo a random walk in energy, with a step size given by equation (77). The number of collisions needed to random walk from $E = -GM/2a_p = -v_p^2/2$ to $E = 0$ is $N \approx 3^{2/3}/16\mu_p^{4/3}$. The probability of a close encounter on each periapse passage is

$$P \approx \frac{\pi r_{\rm H}^2}{(2\pi a_p r_{\rm H})} \approx \frac{1}{2}\left(\frac{\mu_p}{3}\right)^{1/3}. \tag{87}$$

The total number of orbits up to ejection is

$$N_{\rm eject} \approx \frac{3}{8}\mu_p^{-5/3} \approx 4 \times 10^4 \left(\frac{10^{-3}}{\mu_p}\right)^{5/3}. \tag{88}$$

We conclude that particles larger than about 25 μm will be ejected before their orbits are significantly altered by collisions with smaller or similar size dust grains.

4.1.7. *Numerical Results*

We have carried out numerical integrations of test particles in the gravitational field of one or more massive planets orbiting a star. We use the publicly available SWIFT (Levison & Duncan 1994) integration package, which is based on the Wisdom & Holman (1991) symplectic integration scheme. We used the *rmvs3* integrator, in order to integrate through close encounters between the test particles and the planets. All integrations were for 100 million years, with a time step chosen to be small enough to resolve periapse passage for the estimated most extreme test particle orbits or to resolve the perijove passage for planet-grazing close encounters (taken to be at $2r_p$), whichever was smaller. If a particle passed within $2r_p$, it was deemed to have collided with the planet and was removed from the integration.

The initial eccentricities and inclinations (measured from the planet's orbital plane) of the test particles were generally set to 0.1 and 0.087 rad, respectively, although we tried runs with other values. The final ejection velocities did not depend strongly on the initial e and i. The test particles were given semimajor axes ranging from $0.5a_p$ to $1.5a_p$ in single-planet cases, since in those cases particles starting at larger distances from the planet were typically not ejected by the time the integrations were halted.

Figure 5 shows the result of a numerical integration of $\sim$600 test particles in the gravitational field of Jupiter and the Sun. Our analytic calculations should be a good approximation to this case, since $e_{\rm J} = 0.048$. The test particles were started with a range of semimajor axes between x and y, with initial eccentricities $e \sim 0.05$ and inclinations $i \sim 0.05$ rad. The figure shows the velocities at which the particles were

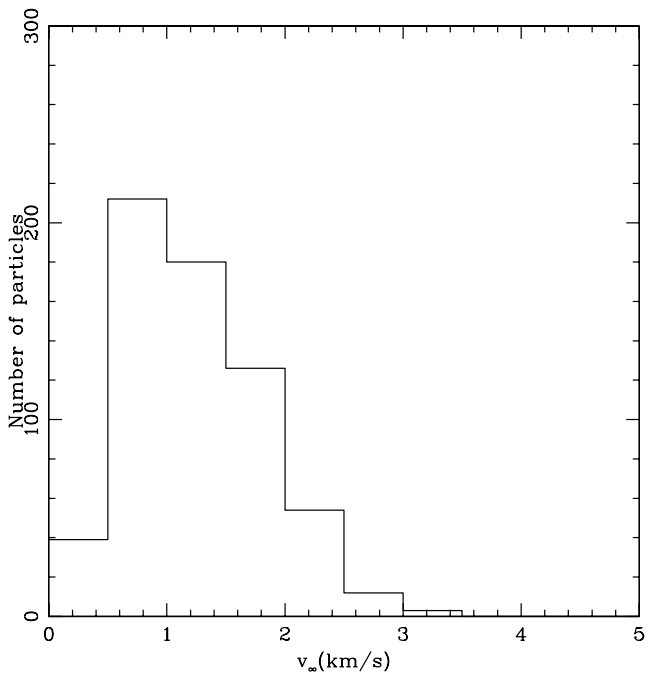

FIG. 5.—Ejection velocities of small particles from a system with a solar-mass star and a Jupiter-mass planet at 5.2 AU.

ejected, including the (small) correction for their finite distance from the Sun when the integration was stopped. The stopping criterion was that the test particle have a positive energy relative to the Sun and a semimajor axis larger than 100 AU. The mean escape velocity is $\sim$1 km s^{-1}, slightly lower than predicted by equation (79).

We found that the final inclinations were small, typically within 10° of the orbital plane of the planet, but with a significant minority of particles ejected at inclinations up to 30°.

We checked the scaling of $v_{\rm ej}$ with a_p by varying the size of the planet's orbit over a decade. A least-squares fit to the mean ejection velocity as a function of a_p gives $v_{\rm ej} \sim a_p^{-0.5}$, with an error of about 0.05 in the exponent. This is consistent with the predicted slope of -0.5 given by equation (78). We also checked the scaling with M_p, finding $v_{\rm ej} \sim M_p^{0.28}$, compared with the predicted exponent of $\frac{1}{4}$. In summary, equations (78) and (79) appear to be a good description of the ejection process.

The numerical integrations employing multiple Jupiter-mass planets gave similar results, with the test particle ejection velocity determined by the most massive of the planets in the integration. The same was true of integrations involving a single Jupiter-mass planet together with several 1–10 Earth mass bodies.

These results suggest that equations (79) and (81) can be used to describe the ejection velocity of small particles in systems with one or more Jupiter-mass planets.

4.2. *Dust Luminosity*

In order to estimate the (age-dependent) dust luminosity of a Vega-like star, we must first estimate the number of grains in the disk. Spangler et al. (2001) have measured IR excesses for stars in several nearby clusters. Their results are consistent with the following relation: dust disk mass $\propto$ (age)$^{-2}$. We normalize this relation by estimating the (size-dependent) number of grains in the disk around β Pic, with an age $\approx$12 Myr (Zuckerman et al. 2001a).

We assume that the grains around β Pic are located at a distance $D = 100$ AU from the star and that they have a size distribution $dN/da = Ca^{-3.5}$, where $N(a)$ is the number of grains with size $\leq a$. This is the equilibrium size distribution that results when mass is redistributed among grain sizes via shattering in collisions (Dohnanyi 1969). We obtain the normalization constant C by setting the emission at 800 μm equal to the observed value of $F_\nu = 115 \pm 30$ mJy (Zuckerman & Becklin 1993). The specific flux is given by

$$F_\nu = \frac{\pi}{D^2} \int da \frac{dN}{da} Q_{\rm abs} a^2 B_\nu[T(a)], \tag{89}$$

where the absorption cross section is $Q_{\rm abs}\pi a^2$, $B_\nu(T)$ is the Planck function, and the grain temperature $T(a)$ is determined by equating the absorption and emission rates. For β Pic, we take effective temperature $T_{\rm eff} = 8200$ K, luminosity $L = 8.7\ L_\odot$, and radius $R = 1.47\ R_\odot$ (Crifo et al. 1997). Grains with $a \gtrsim 1$ cm contribute little to F_ν(800 μm). Terminating the integral in equation (89) at $a = 1$ cm yields $C = 4.65 \times 10^{25}$ cm$^{2.5}$ for silicate grains, implying a disk mass of 1.4×10^{27} g ($\approx$19 lunar masses, 0.23 Earth masses) in grains with $a \leq 1$ cm. If we assume graphite (water ice) rather than silicate composition, then the estimated mass increases by a factor of 1.6 (4.6). Since pure water ice grains are very unlikely, our mass estimate is robust against variations in compositions. If the grains are located 30 pc (500 pc) rather than 100 pc from the star, then the estimated mass decreases by a factor of 2 (increases by a factor of 3). Thus, although the dust actually will be distributed over a range of distances from the star, this does not seriously affect the estimate of the total dust mass.

Our result can be compared with the analysis of Li & Greenberg (1998), who constructed a detailed dust model to account for the emission (at multiple wavelengths) from the dust around β Pic, using fluffy grains. In their model, the total dust mass needed to produce the observed emission is $\sim 2 \times 10^{27}$ g, lying mostly beyond 100 AU from the star.

It is interesting to note that estimates of the dust mass in circumstellar disks typically assume that the grains are in the Rayleigh limit, i.e., that $a \ll \lambda$, the wavelength of the observation (see, e.g., the review by Zuckerman 2001). In this regime, $Q_{\rm abs} \propto a$. In the opposite regime ($a \gg \lambda$), $Q_{\rm abs} \sim 1$. Suppose a_0 is the minimum a for which $Q_{\rm abs} \sim 1$, for fixed λ. Then $Q_{\rm abs} \sim a/a_0$ in the Rayleigh limit. The opacity κ (absorption cross section per unit mass) of the emitting grains is the crucial quantity for estimating dust mass from emission: $\kappa = 3Q_{\rm abs}/4a\rho$. In the Rayleigh limit, $\kappa \sim 3/4a_0\rho$. In our estimate of the dust mass (with our assumption that $dN/da \propto a^{-3.5}$), the emission is dominated by grains with $a \sim a_0$, since these are the most abundant grains with $Q_{\rm abs} \sim 1$. Thus, $\kappa \sim 3/4a_0\rho$ for our estimate, as well as for the Rayleigh limit, and these two different methods yield approximately the same mass in grains contributing significantly to the observed emission. We feel that our scenario, with a Dohnanyi size distribution, is more realistic than the standard scenario, in which all of the grains that contribute significantly to the emission are supposed to be in the Rayleigh limit.

Combining the above estimate for the number of grains in the disk around β Pic with the Spangler et al. (2001) result, we estimate

$$\frac{dN}{da} \sim \left(4.7 \times 10^{25}\ {\rm cm}^{2.5}\right)\left(\frac{12\ {\rm Myr}}{t}\right)^2 a^{-3.5}, \quad a \lesssim 1\ {\rm cm}, \tag{90}$$

where t is the age of the system.

The Spangler et al. (2001) result suggests that grains are lost at a rate $dN/dt \sim -2N/t$. The following could be important sinks for the grains: (1) gravitational ejection from the system, (2) gravitational ejection into the star, (3) incorporation into planets or planetesimals, and (4) ejection of small shattering fragments by radiation pressure. We do not attempt to estimate the relative importance of these sinks in this paper. Rather, we introduce the unknown factor $f_{\rm ej}$, equal to the fraction of the grains that are lost by gravitational ejection. Then the specific dust luminosity is

$$L_{v,a}\left(t, v_{\rm ej}, a\right) = 7.8 \times 10^{18}\ {\rm yr}^{-1}\ {\rm cm}^{-1}\left({\rm cm\ s}^{-1}\right)^{-1} \times \left(\frac{12\ {\rm Myr}}{t}\right)^3 \left(\frac{a}{\rm cm}\right)^{-3.5} f_{\rm ej} f_v(v_{\rm ej}), \tag{91}$$

where we have taken time equal to the age of the star when the grains are ejected and $f_v(v_{\rm ej})dv_{\rm ej}$ is the fraction of the grains ejected with speed between $v_{\rm ej}$ and $v_{\rm ej} + dv_{\rm ej}$.[7]

At very early ages, the primordial gas disk will not yet have dissipated, and the drag force on grains could dramatically reduce the dust luminosity. In addition, we do not expect large

[7] We assume that f_v is independent of a.

grains to be ejected prior to planet formation. Thus, $L_{v,a} = 0$ for $t < t_{\rm cr}$, an unknown critical age. We assume that $t_{\rm cr}$ lies in the range 3–10 Myr.

4.3. *Flux at Earth*

Assuming $f_{\rm survive} = 1$, the flux, at Earth, of grains with size $\geq a$, $F(a)$, is given by

$$F(a) = \left(8.2 \times 10^{-5}\ {\rm yr}^{-1}\ {\rm km}^{-2}\right) f_{\rm beam} f_{\rm ej} \left(\frac{d}{10\ {\rm pc}}\right)^{-2} \times \left(\frac{a}{10\ \mu{\rm m}}\right)^{-2.5} \int dv_{\rm ej} f_v(v_{\rm ej}) \frac{v_{d,\odot}}{v_{\rm ej}} Q\left(t_{\rm ej} = t - \frac{d}{v_{\rm ej}}\right), \quad (92)$$

where

$$Q(t_{\rm ej}) = \begin{cases} \left(\dfrac{12\ {\rm Myr}}{t_{\rm ej}}\right)^3 & t_{\rm ej} \geq t_{\rm cr}, \\ 0 & t_{\rm ej} < t_{\rm cr}. \end{cases} \quad (93)$$

If we assume $v_{d,\odot}/v_{\rm ej} \approx 10$, this yields a flux of $2.6 \times 10^{-21} (25\ \mu{\rm m}/a)^{2.5} (10\ {\rm pc}/d)^2$ cm^{-2} s^{-1}, which may be compared with Figure 1; the AMOR point source supplies a flux at Earth of 10^{-17} cm^{-2} s^{-1}. It would appear that the point source is not due to a debris disk.

We will be interested in sources within the LB, so $f_{\rm survive} = 1$ when $d < r_B$. With $\Phi \approx 0.94$ V and $\rho = 3.5$ g cm^{-3} (appropriate for silicate grains in the LB), equation (45) yields a critical grain radius

$$a_{\rm cr} \equiv (10\ \mu{\rm m}) \left(\frac{d}{9.0\ {\rm pc}}\right)^{1/2} \left(\frac{v}{10\ {\rm km\ s}^{-1}}\right)^{-1/2}. \quad (94)$$

Here $f_{\rm survive} = 1$ when $a > a_{\rm cr}$. We use $v_{*,\odot}$ as a good approximation to $v_{d,\odot}$ in equation (94).

Suppose the threshold of detectability requires 20 events per year, so that the threshold flux $F_{\rm th} = (20\ {\rm yr}^{-1}) A_{\rm col}^{-1}$. Then we can estimate the threshold distance $d_{\rm th}$ out to which sources might be detected by making the optimistic assumptions that $t_{\rm ej} = t_{\rm cr}$ and $f_{\rm ej} = 1$ (we also assume that $f_{\rm beam} = 1$). Inserting equation (94) into equation (92) and assuming $v_{d,\odot}/v_{\rm ej} \sim 10$ yields

$$d_{\rm th} \approx 0.42 \left(\frac{A_{\rm col}}{1\ {\rm km}^2}\right)^{4/13} \left(\frac{t_{\rm cr}}{12\ {\rm Myr}}\right)^{-12/13} {\rm pc}. \quad (95)$$

In Table 3 we give $d_{\rm th}$ and $a_{\rm cr}$ for the cases that $t_{\rm cr} = 3$ or 10 Myr and $A_{\rm col} = 10^4$ or 10^6 km^2; recall that AMOR has $A_{\rm col} \approx 10$ km^2.

Since the flux drops off as $t_{\rm ej}^{-3}$, it is highly advantageous to catch the star when $t_{\rm ej} \sim t_{\rm cr}$. In Figure 6 we plot, as a function of d, the upper and lower ages for which $t_{\rm cr} \leq t_{\rm ej} \leq 2t_{\rm cr}$, assuming a range of ejection speeds between 0.5 and 2 km s^{-1}. Since the total volume and favorable age range both increase with d, distant stars that are possibly too old to have observable IR excesses today may be a significant source population, despite the d^{-2} decrease in flux. However, nearby identifiable Vega-like stars are more attractive sources, since we could then combine the dust flux information with other observations to learn more about a particular object.

TABLE 3
THRESHOLD DISTANCES FOR OBSERVING VEGA-LIKE STARS

$A_{\rm col}$ (km^2)	$t_{\rm cr}$ (Myr)	$d_{\rm th}$ (pc)	$a_{\rm cr}$ (μm)
10^4	3	26	17
10^4	10	8.6	10
10^6	3	108	35
10^6	10	36	20

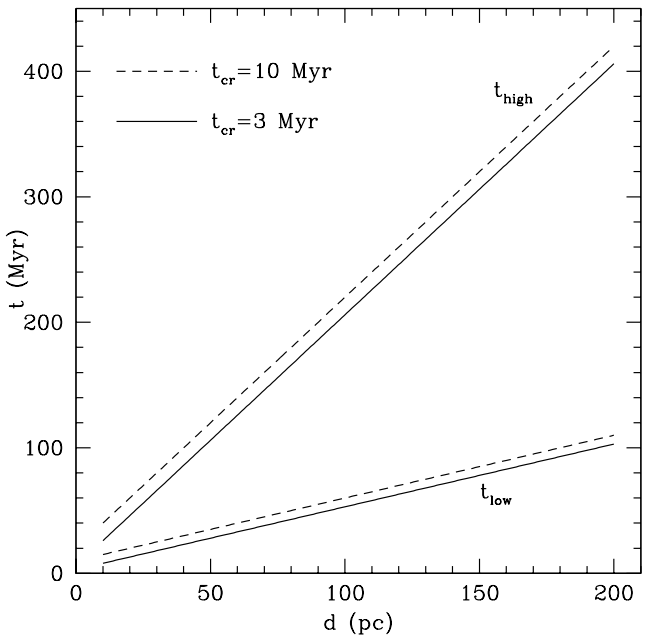

FIG. 6.—Upper and lower current ages t of a Vega-like star for which we would observe grains emitted when the star's age was between $t_{\rm cr}$ and $2t_{\rm cr}$, vs. the distance d to the star.

4.4. *Candidate Sources*

4.4.1. *Gliese Catalog Stars*

Are there any nearby Vega-like stars for which we can expect a detectable dust flux at Earth? To answer this question, we consider stars from the Gliese Catalog with far-infrared excesses from *IRAS* (see Table X in Backman & Paresce 1993).

In Table 4 we give each star's distance d and its space velocity (U, V, W) with respect to the Sun. In calculating these quantities, we have taken coordinates, parallaxes, proper motions, and radial velocities from SIMBAD.[8] We estimate a star's age t from its IR excess τ, which is the fraction of the star's luminosity that is reemitted in the IR by dust. Adopting the Spangler et al. (2001) result that $\tau \propto t^{-2}$, we take

$$t = t(\beta\ {\rm Pic}) \left[\frac{\tau(\beta\ {\rm Pic})}{\tau}\right]^{0.5}. \quad (96)$$

The dust fluxes in Table 4 were calculated using equation (92) with limiting grain size $a = \max(10\ \mu{\rm m}, a_{\rm cr})$ ($a_{\rm cr}$ is taken from eq. [94] with $v = v_{*,\odot}$), a flat distribution of

[8] Note that we exclude one star from Table X in Backman & Paresce (1993), Gl 245, because SIMBAD does not give its radial velocity.

TABLE 4
GLIESE STAR DUST FLUXES

Gl Number	Name	d (pc)	t[a] (Myr)	U[b] (km s^{-1})	V[b] (km s^{-1})	W[b] (km s^{-1})	$v_{*,\odot}$ (km s^{-1})	a_{cr} (μm)	F[c] (yr^{-1} km^{-2})	λ[d] (deg)	β[d] (deg)
68.0.....	DM +19°279	7.5	69.8	34.5	−24.7	2.4	42.5	4.4	3.3E−5	62	33
71.0.....	τ Cet	3.6	170	18.6	29.4	12.7	37.0	3.3	6.3E−6	94	−54
111.0.....	τ^1 Eri	14.0	39.6	−26.2	−16.9	−13.0	33.8	6.8	1.5E−4	262	33
121.0.....	τ^3 Eri	26.4	215	19.4	9.96	−1.09	21.9	11.6	3.4E−8	101	−18
144.0.....	ϵ Eri	3.22	59.7	−3.01	7.22	−20.0	21.5	4.1	1.1E−4	184	8
167.1.....	γ Dor	20.3	107	−22.9	−18.1	−13.8	32.3	8.4	1.2E−6	261	38
217.1.....	ζ Lep	21.5	69.8	−14.4	−11.2	−8.45	20.1	10.9	3.7E−6	260	38
219.0.....	β Pic	19.3	12.0	−10.8	−16.0	−9.11	21.4	10.0	1.5E−3	268	51
248.0.....	α Pic	30.3	194	−35.4	−19.3	−10.1	41.6	9.0	1.0E−7	268	25
297.1.....	B Car	21.4	31.4	19.8	−15.1	−34.0	42.2	7.5	1.1E−3	140	48
321.3.....	δ Vel	24.4	351	11.6	−1.15	−5.00	12.7	14.6	2.3E−9	107	17
364.0.....	DM −23°8646	14.9	69.3	−39.9	−25.4	6.27	47.7	5.9	1.4E−5	290	17
448.0.....	β Leo	11.1	135	−20.1	−16.1	−7.80	26.9	6.8	1.2E−6	268	36
557.0.....	σ Boo	15.5	123	2.06	15.9	−5.17	16.9	10.1	5.7E−7	165	−38
673.1.....	DM −24°13337	25.7	34.5	−35.8	−13.1	−11.6	39.9	8.5	6.4E−4	261	20
691.0.....	μ Ara	15.3	58.8	−13.7	−8.39	−3.97	16.5	10.1	9.7E−6	270	26
721.0.....	α Lyr	7.76	152	−16.1	−6.33	−7.76	18.9	6.7	1.1E−6	256	26
820.0.....	61 Cyg	3.48	48.0	−93.8	−53.4	−8.33	108	1.9	1.0E−3	278	23
822.0.....	δ Eql	18.5	80.0	5.72	−28.6	−10.3	30.9	8.2	4.3E−6	18	78
881.0.....	α PsA	7.69	83.1	−5.70	−8.22	−11.0	14.9	7.6	5.7E−6	235	54

[a] Age of star from eq. (96).
[b] Space velocity of the star relative to the Sun; U is positive toward the Galactic center, V is positive along the direction of the Galactic rotation, and W is positive toward the north Galactic pole.
[c] Dust flux calculated using eq. (92) with a limiting grain size $a = 10$ μm, a flat distribution of ejection velocities between 0.5 and 3 km s^{-1}, $t_{cr} = 3$ Myr, and $f_{survive} = f_{beam} = f_{ej} = 1$.
[d] Apparent location of dust stream on the sky; λ is ecliptic longitude and β is ecliptic latitude. In most cases, $v_{ej} = 1$ km s^{-1} is adopted; for Gl 219.0 (β Pic) $v_{ej} = 3$ km s^{-1} is adopted, since the dust will not yet have reached us if $v_{ej} = 1$ km s^{-1}.

ejection velocities between 0.5 and 3 km s^{-1}, $t_{cr} = 3$ Myr, and $f_{beam} = f_{ej} = 1$. Thus, these estimates are optimistic. In § 7 we suggest how to build a radar detector with $A_{col} \approx 3 \times 10^4$ km^2. Four of the stars in Table 4 would yield 20 or more meteors per year (i.e., $F > 6 \times 10^{-4}$ yr^{-1} km^{-2}) for such a system. Since t_{ej} is substantially greater than t_{cr} for most of the stars, increasing t_{cr} to 10 Myr yields reduced fluxes for only three stars: Gl 219, Gl 297.1, and Gl 673.1. The flux for Gl 219 (β Pic) vanishes, whereas the fluxes for Gl 297.1 and Gl 673.1 remain greater than 2×10^{-5} yr^{-1} km^{-2}.

The apparent location of a dust source on the sky is determined by the velocity of the dust relative to the Sun (eq. [4]). If the dust ejection speed v_{ej} were much greater than the star's speed $v_{*,\odot}$, then the dust would appear to come from the location of the star itself (since the speed of light is much greater than the star's speed). However, v_{ej} is typically an order of magnitude or more smaller than $v_{*,\odot}$. Thus, the location of the dust source on the sky is primarily determined by $\boldsymbol{v}_{*,\odot}$ and need not be anywhere near the actual location of the source.

Since $\boldsymbol{v}_{*,\odot}$ is determined in part by the velocity $\boldsymbol{v}_{\odot,LSR}$ of the Sun relative to the local standard of rest (LSR), we may expect some degree of clustering of the apparent directions around the solar apex (i.e., the direction of $\boldsymbol{v}_{\odot,LSR}$). Dehnen & Binney (1998) give $U = 10.00 \pm 0.36$ km s^{-1}, $V = 5.25 \pm 0.62$ km s^{-1}, and $W = 7.17 \pm 0.38$ km s^{-1} for $v_{\odot,LSR}$. They find that the velocity of the Sun with respect to nearby young stars is similar, except that $V \approx 12$ km s^{-1} in this case. The coordinates of the solar apex with respect to the LSR are $(l, b) = (27\overset{\circ}{.}7,\ 32\overset{\circ}{.}4)$ or $(\lambda, \beta) = (248\overset{\circ}{.}4,\ 32\overset{\circ}{.}2)$, while those with respect to nearby young stars are $(l, b) = (50\overset{\circ}{.}2,\ 24\overset{\circ}{.}7)$ or $(\lambda, \beta) = (265\overset{\circ}{.}7,\ 48\overset{\circ}{.}9)$. In addition to Galactic coordinates (l, b), we also make use of ecliptic coordinates: ecliptic longitude λ and ecliptic latitude β. These coordinates are useful in radar studies of meteors because most of the observed grains originate in the ecliptic plane. In Table 4 we give the apparent direction to the dust stream in ecliptic coordinates. Figure 7 is a plot of these directions on the sky.

4.4.2. *Young Clusters*

Nearby young clusters could potentially yield strong dust fluxes. The cluster members may not have appeared in searches for the Vega phenomenon, since the stellar luminosities may be too low. However, most nearby clusters have poor tuning between distance and age. There are some very young clusters that are too far away for the dust to have reached us yet and some nearer clusters that are much older (see Table 1 in Spangler et al. 2001).

The recently discovered Tucana association (Zuckerman, Song, & Webb 2001b) might be more suitable. Zuckerman & Webb (2000) find a distance $\sim$45 pc, age $\sim$40 Myr, and space velocity $(U, V, W) \approx (-11,\ -21,\ 0)$ km s^{-1}. Stelzer & Neuhäuser (2000) find a younger age of 10–30 Myr. Adopting numbers from Zuckerman & Webb (2000) and making use of the convenient coincidence that 1 km s^{-1} = 1.02 pc Myr^{-1}, we find that dust ejected at speed $v_{ej} = 1.5$ km s^{-1} when the stars were 15 Myr old would be reaching us today. The position of the dust stream on the sky would be $(\lambda, \beta) = (126^\circ,\ -46^\circ)$.

The Pleiades cluster is another potential source, with a distance of 118 pc and an age of $\approx$120 Myr (Spangler et al. 2001). Although the large distance would suppress the flux (because of both the d^{-2} dependence in eq. [92] and the need for larger grains in order to avoid magnetic deflection), this could be partially compensated by the large number of stars in

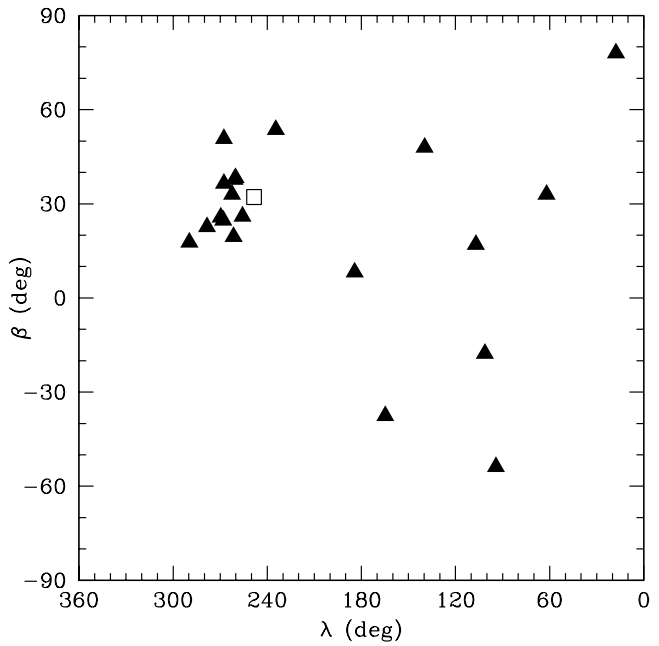

FIG. 7.—*Triangles*: Apparent locations of the dust flux from the Gliese stars in Table 4. *Open square*: Direction of the solar apex. Coordinates are ecliptic longitude (λ) and latitude (β).

the cluster. Robichon et al. (1999) find $(U, V, W) = (-6.35, -24.37, -13.02)$ km s^{-1} for the cluster motion. Ignoring the Galactic potential, this would yield $(\lambda, \beta) \approx (276^\circ, 73^\circ)$ for the position of the dust stream.

4.5. *Has Dust from β Pic Been Detected?*

Baggaley (2000) detected a "discrete" source of radar meteoroids with a central location $(\lambda, \beta) \approx (280^\circ, -56^\circ)$, an angular diameter of $\sim 30^\circ$, and a dust speed relative to the Sun $v_{d,\odot} \approx 13$ km s^{-1}. He claimed that the central location and dust speed could be reproduced if β Pic were the source and the grains were ejected with speed $v_{ej} \approx 29$ km s^{-1}.

This result seems unlikely on theoretical grounds, since it is not clear how the grains can be ejected with such large speeds. In addition, we do not find that dust emitted from β Pic reproduces the location of the discrete source for any v_{ej}. Baggaley did his calculations in the LSR frame, taking the Sun's motion with respect to the LSR from Binney & Tremaine (1987), who give $(U_\odot, V_\odot, W_\odot) = (9, 12, 7)$ km s^{-1}. Baggaley found the direction to the discrete source to be $(\lambda, \beta) = (49^\circ, -72^\circ)$, $(l, b) = (259^\circ, -28^\circ)$, whereas we find $(\lambda, \beta) = (58.^\circ6, -81.^\circ3)$, $(l, b) = (267.^\circ4, -34.^\circ1)$. Note that the two coordinate pairs given by Baggaley do not actually correspond to the same point on the sky.

In Figure 8 we plot the sky position of a dust stream emitted by β Pic for various values of v_{ej} (*triangles*). The filled square indicates the central location of Baggaley's discrete source. For reasonable ejection speeds ($v_{ej} \lesssim 3$ km s^{-1}), the location of the dust stream differs dramatically from that of the discrete source. For $v_{ej} \approx 30$ km s^{-1}, the locations are much closer and $v_{d,\odot} \approx 13$ km s^{-1}. Although the dust stream does lie within the $\sim 30^\circ$ extent of the source in this case, it is still 12° away from the center of the source.

The particle flux coming from the discrete source is several orders of magnitude larger than we would expect from a debris disk at 20 pc. From equation (92) we find that β Pic produces a flux of $a = 10$ μm particles of 10^{-3} km^{-2} yr^{-1} at Earth. Given our estimate of the collecting area of the AMOR detector, somewhat less than 10 km^2, AMOR is not capable of detecting such a low flux.

Thus, it appears that Baggaley's discrete source is not related to β Pic.

4.6. *Potential Distributed Sources*

In addition to the discrete source, Figures 2*b* and 2*c* in Baggaley (2000) suggest the presence of a distributed, band-like feature. Here we discuss three possible sources for a distributed feature, namely, the Galactic plane, the Gould Belt, and the spiraling of grains in the local magnetic field.

4.6.1. *The Galactic Plane*

The scale height of young stars above the Galactic plane is $\sim$90 pc (Gilmore & Reid 1983). Thus, we might expect to see a signature of the plane in the dust flux since we can detect grains from sources beyond 100 pc if a and v are large enough (but v must not be so large that the grains are destroyed). The effects of the Galactic gravitational potential cannot be ignored for such large distances, but we do not expect the Galactic potential to deflect grains out of the plane. As mentioned in § 4.4.1, the apparent direction of a dust stream with a low ejection speed is primarily determined by the velocity of the source with respect to the Sun. Since the Galactic plane is a feature in physical space rather than velocity space, it may seem that it should not actually appear as a band on the sky in a dust flux map. However, if the radial velocity of a source (with respect to the Sun) exceeds the dust ejection speed, then, unless the source passed near the current location of the Sun at some time in the past, the dust will never reach the Sun. Thus, although the velocity of the source with respect to the Sun determines the direction of the dust stream, the location of the

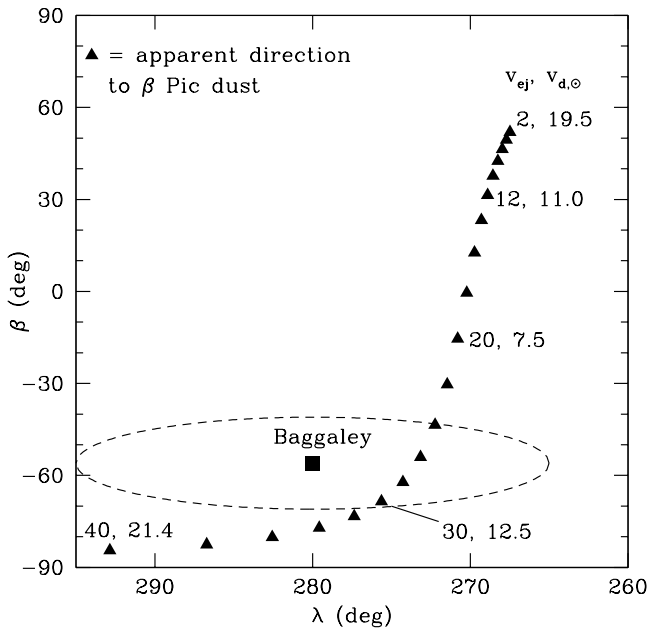

FIG. 8.—Filled square marks the central location of the discrete source observed by Baggaley (2000), and the dashed line indicates its extent. Triangles mark the apparent location of a dust stream from β Pic for values of the ejection speed v_{ej} ranging from 2 to 40 km s^{-1} in steps of 2 km s^{-1}. For a few cases, v_{ej} and the speed of the dust with respect to the Sun, $v_{d,\odot}$, are indicated. The ecliptic coordinates of β Pic itself are $(\lambda, \beta) = (82.^\circ5, -74.^\circ4)$.

source does restrict which velocities can give rise to an observable dust stream.

From equations (92) and (94), the dust flux $F \propto d^{-3.25}$, so it is not clear that distant stars in the plane can indeed produce a noticeable band on top of the relatively isotropic distribution produced by nearby stars. The following simple estimate shows that a band is expected, although at a low contrast level. For stars with distance $R < 90$ pc, the volume element (in which young stars are found) is $dV = 4\pi R^2\, dR$, while $dV = (90\text{ pc})2\pi R\, dR$ for $R > 90$ pc. Thus, the ratio of the flux $F_{\rm plane}$ due to the Galactic plane to the isotropic flux $F_{\rm iso}$ (due to nearby stars) is

$$\frac{F_{\rm plane}}{F_{\rm iso}} \approx \frac{(180\text{ pc})\pi \int_{90\text{ pc}}^{\infty} dR\, R^{-1.25}}{4\pi \int_{0}^{90\text{ pc}} dR\, R^{-0.25}} = 1.6, \qquad (97)$$

where we have multiplied each integrand by a factor R to account for the increased probability of catching a star when $T_{\rm ej} \approx T_{\rm cr}$.

Since the components of random stellar velocities perpendicular to the plane are smaller than those parallel to the plane, the Galactic plane should appear as a fuzzy band on the sky even considering only stars closer than 90 pc.

Note that the observed dust flux band should be warped in such a way as to favor the direction of the solar apex.

4.6.2. *The Gould Belt*

The Gould Belt is a band on the sky, inclined $\approx 20^\circ$ with respect to the Galactic plane and with an ascending node $l_\Omega \approx 280^\circ$, along which young stars tend to lie (for reviews see Pöppel 1997; de Zeeuw et al. 2001). From a *Hipparcos* study of early-type stars, Torra, Fernández, & Figueras (2000) concluded that ≈60% of the stars younger than 60 Myr and within 600 pc of the Sun are in the Gould Belt. OB associations, young star clusters, and molecular clouds have long been known to trace the Gould Belt. Recently, Guillout et al. (1998) detected late-type stellar members of the Gould Belt population, by cross-correlating the *ROSAT* All-Sky Survey with the Tycho catalog. Thus, the Gould Belt could be responsible for a distributed grain flux feature.

Guillout et al. (1998) found that the three-dimensional structure of the Gould Belt is disklike. The outer rim of the Gould Disk is ellipsoidal, with a semimajor axis of ≈500 pc and a semiminor axis of ≈340 pc. The center of the structure is ≈200 pc from the Sun, toward $l \approx 130^\circ$. On the near side ($l \approx 310^\circ$), the inner edge of the Gould Disk lies only ≈30 pc from the Sun, although most of the young stars lie beyond ≈80 pc.

Estimates of the age of the Gould Belt range from 20 to 90 Myr (for a review see Torra et al. 2000); Torra et al. (2000) favor an age between 30 and 60 Myr. Grains traveling with $v_{\rm ej} = 1.5$ km s^{-1} reach a distance of ≈90 pc from their star of origin in 60 Myr. Thus, only the near side of the Gould Disk should be visible in the dust flux.

The kinematics of the Gould Belt is still poorly understood, but it is clear that the member stars are undergoing some sort of expansion. If the expansion dominates the random velocities, then the near side of the Gould Belt should appear on the opposite side of the sky in the dust flux, i.e., centered on $l \approx 130^\circ$. If the random velocities are more important, then we would expect to see a feature lying in the same direction as the near side of the Gould Belt, as a result of stars moving toward us.

4.6.3. *Spiraling of Grains in the Local Magnetic Field*

Thus far, we have only considered grains that are not dramatically deflected as they travel from their source to Earth. Suppose the magnetic field were uniform throughout the LB. In this case, deflected grains would produce a wide band centered on the plane perpendicular to the field. The actual field presumably includes a significant random component, so the resulting distributed feature (if any) may be more complicated than a wide band.

5. DUST FROM AGB STARS

Stars with main-sequence mass $M \lesssim 6\, M_\odot$ spend time on the AGB. During this evolutionary phase, a wind is driven off the star, with mass-loss rates as high as $\sim 10^{-5}\, M_\odot$ yr^{-1}. Grain formation in these outflows likely supplies a large fraction of the dust in the ISM. See Habing (1996) for a general review of AGB stars.

Since the grains spend only a limited time in a high-density environment, the size distribution of the newly formed dust is thought to be dominated by grains with $a < 1$ μm (see, e.g., Krüger & Sedlmayr 1997). Observations confirm the significant presence of submicron grains. Jura (1996) examined the extinction due to circumstellar dust around seven O-rich giants and found that it rises toward the ultraviolet. From observations of scattering, Groenewegen (1997) found a mean grain size $a \approx 0.16$ μm for the circumstellar envelope of the carbon star IRC +10216.

Even if submicron grains dominate the outflows from AGB stars, the luminosity of grains with $a \gtrsim 10$ μm may be high enough to result in detectable fluxes at Earth, since the dust production rate is so high. Grains with isotopic ratios indicative of formation in AGB stars have been discovered in meteorites. Although most of these grains have $a \sim 0.5$ μm, some are as large as $a \approx 10$ μm (Zinner 1998).

Suppose that the grains all have radius a and that a total dust mass M_d is emitted during the AGB lifetime τ. The dust luminosity is then $L = 3M_d/(4\pi\rho a^3\tau)$. We adopt $M_d \sim 0.01\, M_\odot$ and the canonical lifetime $\tau \sim 10^5$ yr (Habing 1996). The flux at Earth follows from equation (3). For simplicity, we take $f_{\rm beam} = 1$ and $f_{\rm survive} = 1$; also, since the typical grain ejection speed in an AGB wind is ~ 10 km s^{-1} (Habing 1996), we take $v_{d,\odot}/v_{\rm ej} = 1$. Thus, the flux as a function of AGB star distance d is approximately

$$F(d) \sim (114\text{ yr}^{-1}\text{ km}^{-2})\left(\frac{M_d}{10^{-2}\, M_\odot}\right)\left(\frac{\rho}{3.5\text{ g cm}^{-3}}\right)^{-1} \times \left(\frac{a}{10\ \mu\text{m}}\right)^{-3}\left(\frac{\tau}{10^5\text{ yr}}\right)^{-1}\left(\frac{d}{100\text{ pc}}\right)^{-2}. \qquad (98)$$

In order for the grains to be traceable to their point of origin, we require that the gyroradius $r_B > d$. This yields a minimum acceptable grain size (eq. [45]), so that

$$F(d) \lesssim (8\text{ yr}^{-1}\text{ km}^{-2})\left(\frac{M_d}{10^{-2}\, M_\odot}\right)\left(\frac{\rho}{3.5\text{ g cm}^{-3}}\right)^{1/2}\left(\frac{\Phi}{0.5\text{ V}}\right)^{-3/2} \times \left(\frac{B}{5\ \mu\text{G}}\right)^{-3/2}\left(\frac{v}{10\text{ km s}^{-1}}\right)^{3/2}\left(\frac{\tau}{10^5\text{ yr}}\right)^{-1}\left(\frac{d}{100\text{ pc}}\right)^{-7/2}. \qquad (99)$$

The above flux is for the optimistic case that all of the dust mass is in the smallest grain size a_t (25 μm in this case) such that the grain will barely be undeflected. In cgs units, this flux is 2.5×10^{-17} cm^{-2} s^{-1}, tantalizingly close to the flux of the point source seen by Baggaley (2000).

Jackson, Ivezić, & Knapp (2002) have studied the distribution of AGB stars with mass-loss rates in the range 10^{-6} to $10^{-5}\,M_\odot$ yr^{-1}. They find that the number density of AGB stars $n_{\rm AGB} \approx 4.4 \times 10^{-7}$ pc^{-3} in the solar neighborhood. Thus, the number of sources within a distance d from the Sun is $N(d) \approx 1.84(d/100\ {\rm pc})^3$.

In Table 5 we give the flux F from equation (99) and the number N of sources for a few values of d. We also give the threshold grain size a_t and the fraction g of the emitted dust mass that would need to be in such large grains in order to yield an observed flux at Earth of 2×10^{-3} yr^{-1} km^{-2} (corresponding to 20 events per year with a collecting area of 10^4 km^2). We see from the table that AGB stars could be a significant source population for radar detection of extrasolar meteoroids if a small fraction of the grains in the outflow are large. Note that the source AGB star will not be visible as such, as a result of the large distances to AGB stars and their short lifetimes. In addition, the distances are large enough that the grain trajectories will be affected by the Galactic potential.

Even if all the grains in the AGB outflow are smaller than 10 μm, there is still a chance to see the AGB star as a source on the sky, since some AGB stars apparently have long-lived disks in which grain coagulation occurs. This phenomenon has been observed for binary stars; the presence of the companion apparently causes some of the outflowing grains to be deflected into a disk. A well-studied example is AC Her (Jura, Chen, & Werner 2000). Jura et al. (2000) find that the grains must have $a \gtrsim 200$ μm in order to remain gravitationally bound, as a result of the extreme luminosity of the evolved star. They estimate the mass of the dust disk (in grains with $a \lesssim 0.1$ cm) to be $\approx 1.2 \times 10^{30}$ g. Their observations of infrared emission imply the presence of much smaller grains as well. They suggest that shattering during collisions between disk grains leads to a radiation pressure–driven outflow of smaller grains. The lifetime of such disks and the frequency with which they occur remain unknown. The large disk mass suggests the possibility of very large dust fluxes, and the commonality of binaries suggests that the frequency could be high. Other examples of stars with circumbinary disks are HD 44179 (the central star of the Red Rectangle nebula; Jura, Turner, & Balm 1997), IRAS 09425−6040 (Molster et al. 2001), and SS Lep, 3 Pup, and BM Gem (Jura, Webb, & Kahane 2001).

If the AMOR point source is (or was) an AGB star, the star would currently be a young, hot, high proper motion white dwarf. The proper motion would point back to the vicinity of the AMOR source, after allowing for the uncertain aberration of the dust particles.

6. DUST FROM YOUNG STELLAR OBJECTS

The accretion of material onto a forming star is accompanied by a bipolar outflow of material. These outflows appear as both highly collimated, supersonic ($v \sim 100$−200 km s^{-1}) jets and large-angle molecular outflows (with $v \lesssim 25$ km s^{-1}; for reviews see Reipurth & Bally 2001; Königl & Pudritz 2000; Shu et al. 2000; Eislöffel et al. 2000; Richer et al. 2000).

The mechanism for launching the outflow is not yet well understood. If the material originates in the disk and if the density is high enough, then large grains can be entrained in the outflow, assuming that there has been sufficient time for growth to large sizes. As the density decreases, the grains decouple from the gas and retain their launching speed, which could be $\sim$10–500 km s^{-1}. Chugai (2001) has appealed to the ejection of large grains from YSOs to explain the early AMOR detections of interstellar meteors (Taylor et al. 1996). He finds that the flux supplied from YSOs is a factor of 30 below that claimed by the AMOR group.

Shocks form when the jets run into the ambient ISM, and grains could be destroyed in the shocked regions (known as Herbig-Haro objects). Observations have yielded contradictory results on this point. Beck-Winchatz, Böhm, & Noriega-Crespo (1996) and Böhm & Matt (2001) find that the gas-phase Fe abundance in Herbig-Haro objects is generally close to solar, indicating very efficient grain destruction. Mouri & Taniguchi (2000), on the other hand, find the gas-phase Fe abundance to be ≈20% solar, indicating only a modest amount of grain destruction. Grain destruction is not expected for the slower, wide-angle outflows. However, these outflows may consist of ambient material swept up by the jets (Königl & Pudritz 2000), in which coagulated grains might not be present. Thus, it is not yet clear whether or not YSO outflows contain large grains.

We can make an optimistic estimate of the dust luminosity by assuming that $\sim$1% of the outflowing mass is in large grains, as we did for AGB stars. The mass-loss rate can be as high as $\sim 10^{-6}\,M_\odot$ yr^{-1} (Eislöffel et al. 2000), yielding a flux

$$F(d) \approx 2.8 \times 10^{-18} \left(\frac{100\ {\rm pc}}{d}\right)^2 \frac{v_{d\odot}}{v_{\rm ej}}\ {\rm cm}^{-2}\ {\rm s}^{-1}, \qquad (100)$$

where we have assumed $a = 25$ μm. For ejection in a jet, this is ≈100 times smaller than the optimistic estimate for an AGB star at the same distance. However, the space density of YSOs is larger than that of AGB stars; TW Hydrae, a T Tauri

TABLE 5
AGB Star Dust Fluxes

d[a] (pc)	F[b] (yr^{-1} km^{-2})	N[c]	a_t[d] (μm)	g[e]
100.....	7.99	1.84	24.3	2.50E−4
200.....	0.706	14.7	34.3	2.83E−3
500.....	2.86E−2	230	54.2	6.99E−2

[a] Distance to AGB star.
[b] Flux from eq. (99).
[c] Number of AGB stars within distance d from Sun.
[d] Threshold grain size for traceability to source.
[e] Fraction of emitted grains that must have $a > a_t$ in order for flux at Earth to equal 2×10^{-3} yr^{-1} km^{-2}.

star, is only 59 pc from the Sun and is associated with dozens of other young stars at similar distances. There is good evidence that TW Hydrae has a $\sim$100 km s^{-1} wind (Herczeg et al. 2002; Wilner et al. 2000). TW Hydrae may be associated with the Gould Belt (Makarov & Fabricius 2001). While the (optimistic) flux estimate given here is lower by a factor of order 100 than is realistically detectable by AMOR, TW Hydrae and stars associated with it might be seen by more sensitive future radar systems.

The outflow may last $\sim 10^6$ yr, 10 times longer than the AGB star lifetime. In the following stage of evolution, the YSO disk is dispersed, perhaps by photoevaporation. In this phase, the mass-loss rate could be as high as $\sim 10^{-7}\, M_\odot$ yr^{-1} (Hollenbach, Yorke, & Johnstone 2000), yielding a maximum dust luminosity 10 times lower than for the bipolar outflows.

Given the potentially large dust luminosities, YSOs could be likely candidate sources for extrasolar meteoroids. However, the young stars listed in Table 4 are probably too old, given their proximity. For example, if disk dispersal is complete at an age of 3 Myr, then dust from the YSO phase of β Pic has been traveling for $\approx$9 Myr. At a speed of 10 km s^{-1}, the dust would now be $\approx$90 pc from β Pic, but the Sun is only $\approx$20 pc from β Pic. If, however, disk dispersal continues until an age of 10 Myr, then β Pic may appear as a YSO dust source today.

Some nearby, young clusters could produce large total fluxes distributed over a wide area on the sky. Such clusters include TW Hydrae ($d \sim 55$ pc, $t \sim 10$ Myr; Zuckerman & Webb 2000), Upper Scorpius ($d \sim 145$ pc, $t \sim 1-10$ Myr; Spangler et al. 2001), Chamaeleon Ia and Ib ($d \sim 140-150$ pc, $t \sim 1-40$ Myr; Spangler et al. 2001), and Taurus ($d \sim 140$ pc, $t \sim 10-40$ Myr; Spangler et al. 2001).

7. DISCUSSION

Our calculations suggest that there are a number of nearby sources of 10 μm or larger particles that yield sufficient fluxes to be detectable by ground-based radar systems. Here we suggest ways to optimize radar systems for meteor detection.

Meteoroids with $a \lesssim 10$ μm cannot travel through the ISM for appreciable distances. Furthermore, it appears that the flux of meteoroids decreases with increasing meteoroid size. It follows that if one is interested in detecting particles from an identifiable source, large radar collecting area is more crucial than large radar power, once the power is sufficient to detect $a \approx 10$ μm particles.

The returned radar power falls off as $1/R^3$ for radars that detect coherent emission from a substantial fraction of the meteor trail (such as AMOR), or as $1/R^4$ for meteor head detectors such as Arecibo. The minimum range to the meteor trail is given by the height of the trails (of order 100 km), while the maximum range is of order 1000 km as a result of the curvature of Earth. Increasing the mean range by a factor of 10 will increase the collecting area, and hence the flux, by a factor of 100 but requires an increase in radar power by a factor of 10^3 to 10^4, depending on the type of radar employed. While the cost of a high-power radar transmitter increases rapidly with increasing power, it is clearly helpful to maximize the transmitted power.

Another way to increase the radar range, and hence the collecting area, is to increase the gain of the antenna; the received power scales as the product $G_T G_R$. However, there are limits to the extent to which one can increase the antenna gain. If the radar is like AMOR, the width of the beam must exceed the length of a typical meteor trail, or else the number of coherently emitting electrons will drop. The angular width of the trail is of order H_p/R, which ranges from 0.06 to 0.006 rad, or from 3° (in right ascension, if the beam looks due south or north) at the zenith to 0.°3 at the horizon. Optimally, the beam will cover the sky from the zenith to the horizon, so the antenna gain should be no larger than $\sim$1000.

Selecting a gain of this magnitude matches the beam size to the length of the meteor trail but limits the geometric area A_G of the antenna, partially defeating the purpose, which is to maximize the collecting area. This is the case with AMOR, where the choice of a narrow beam was dictated by the need for high-precision measurement of the meteor position, but at the cost of collecting area. To get around this problem, we propose building an array of antennas, all powered by the same radio generator. The beams of the array would all have widths of order 3°, but the beams would be directed around the points of the compass. In principle, one could have $\sim$100 such beams emanating from a single facility. The duration of a radar pulse is typically a microsecond, while the time between pulses is of order a millisecond. (The time to travel out and back 1000 km is about 6 ms; in that time the meteoroid will travel a distance $\sim$240 m.) One could send out pulses, directed at different points around the compass, separated by 10 ms. The receiver would be turned off when the transmitter is on, about 10^{-4} of the time. Return pulses from trails at different compass points would overlap in time, but given sufficient receiver gains, cross talk between the receivers should be small enough to be acceptable.

If one employs a sufficiently powerful radar, one can live with a low antenna gain and still achieve large collecting area. However, the need for high-precision determinations of the meteor positions remains. This problem can be addressed by using separate transmitting and receiving antennae. The transmitter can have a broad beam, with a low gain but covering a large fraction of the sky. An antenna array can then be used as an interferometer to locate the meteor on the sky.

Either a multibeam radar or single broad beam radar with an interferometer could have a collecting area $A_{\rm col}$ of order 800 km^2, if the typical range were $R \sim 150$ km. Current distant early warning (DEW) radar may be interesting in this context. The existence of tens of such systems, with an aggregate collecting area of $\sim$10,000 km^2, only adds to their attractiveness as extrasolar meteor detectors.

The collecting area grows dramatically, up to 35,000 km^2, if the radar can detect 10 μm particles out to the horizon. This is 4000 times the collecting area of the AMOR radar. AMOR sees about 10 extrasolar meteors every day; the proposed detector would see up to 40,000 extrasolar meteoroids of size 35 μm per day and about 10^6 10 μm extrasolar meteoroids per day. This suggests that one of the major constraints is handling the data, since there would be of order 10^9 interplanetary dust particles detected per day.

Such a radar would be capable of detecting meteoroids from a handful of nearby debris disks; Table 4 lists four nearby young Gliese stars that might have fluxes exceeding 6×10^{-4} particles per year per square kilometer. This large-area radar system would also detect meteoroids from (former) AGB stars with fluxes as low as 2×10^{-11} cm^{-2} s^{-1}; in the optimistic case that a substantial fraction of emitted particles have $a \gtrsim 25$ μm, sources as distant as a kiloparsec could be seen. From Table 5 this could be several hundred stars. The number of possible YSO sources could be somewhere between these two estimates.

How feasible is such a radar? We have already mentioned the current DEW systems. However, we note that moderate enhancements to an AMOR-type radar are all that are needed.

The product of the transmitter and receiver gain could be enhanced by a factor of 5–10, while the power could be enhanced by a factor of 20, to 2 MW, for a total increase in received power of a factor of $\sim$200. This would allow for the detection of $a = 10$ μm size particles at ranges of $\sim$500 km. Further progress could be made by increasing the operating wavelength; a factor of 2 increase, to $\lambda = 2000$ cm, would be sufficient to detect 10 μm size particles out to the horizon.

The flux of interstellar meteoroids of different mass appears to follow a power law $mf_m \propto m^{-1.1}$, over five decades in mass. This may be compared to the Dohnanyi law, $f_m \propto m^{-\alpha}$, with $\alpha = 11/6 \approx 1.83$; in the case of interstellar meteoroids, $\alpha \approx 2.1$. We note that the observed size distribution of asteroids has $\alpha \approx 2$ for objects larger than $a = 2.5$ km and $\alpha \approx 1.4$ for a between 2.5 and 0.1 km (Ivezić et al. 2001). However, the binding energy per gram can be expected to vary with size, a fact we appealed to in explaining the observation that meteoroids of very difference sizes ablate at the same height in Earth's atmosphere. In our view, the rough agreement between the values of α might reflect a common origin in a collisional cascade but is more likely a coincidence.

Krivova & Solanki (2003) recently suggested that interactions with a Jupiter-mass planet could eject dust grains with velocities of order 10–70 km s^{-1}. They cited this result as support for the identification of the point source found by Baggaley (2000) with β Pic. Our analytic calculations show that only a tiny fraction of ejected particles will have such high velocities, a result supported by direct numerical integrations.

8. CONCLUSIONS

We have provided simple analytic estimates for the minimum size of radar-detected meteoroids as a function of radar power and antenna gain. We give very rough estimates of the collecting area of radar detectors, and hence of fluxes of interstellar meteoroids, assuming that the claimed detection rates are correct. The fluxes of satellite- and radar-detected interstellar meteoroids appear to lie along a power law, $mf_m \propto m^{-1.1}$, corresponding to $\alpha = 2.1$, or a size scaling $\gamma = 4.3$, in contrast to the Dohnanyi value $\gamma = 3.5$.

We examine three possible sources of large, $a > 10$ μm size extrasolar meteoroids. In descending order of dust luminosity, they are AGB stars, YSOs (with winds and/or jets), and debris disks. (Supernovae can supply similar mass fluxes of particles, but we expect the particles to be smaller.) We show that such large particles can travel in straight lines for tens of parsecs through the ISM, which in principle will allow their sources to be traced.

Since there are approximately two AGB stars within 100 pc of the Sun at any time, we expect that there will be approximately two sources of extrasolar meteoroids, with fluxes at Earth approaching $\sim$8 yr^{-1} km^{-2}, on the sky at all times. Such a star might be responsible for the "point source" reported in Baggaley (2000). The AMOR radar, according to our estimates, is marginally capable of detecting such a small flux. The star itself would currently be a hot white dwarf with a high proper motion, within $\sim$100 pc of the Sun.

There is one known T Tauri star within 100 pc of the Sun, TW Hydrae. This star has a high-velocity outflow ($\sim$100 km s^{-1}) from a dusty disk. It is very likely expelling 10–100 μm size particles; unfortunately, the flux is clearly too small, by a factor of $\sim$100, to be detected by current radar systems.

Similarly, currently known debris disk systems provide fluxes that are too small to be detected at present. We have shown that the system implicated by Baggaley (2000), β Pic, is unlikely to provide a particle flux as large as that associated with his point source. We also show that the location of the apparent source on the sky is inconsistent with particles ejected from β Pic by gravitational interaction with a Jupiter-mass planet in the system; we showed that typical ejection velocities in that case are of order 1 km s^{-1}. Even if the ejection velocity is assumed to be 30 km s^{-1}, the most favorable value, the apparent position of the source does not match the observed position (see Fig. 8). Since the particle flux, ejection velocity, and position on the sky do not match the observations, we conclude that the point source is not associated with gravitational ejection from the debris disk of β Pic.

However, we would like to stress that all three types of sources, AGB stars, YSOs, and debris disks, should be detectable by future ground-based radar systems. The pioneering AMOR system may have already detected meteoroids from an AGB star. Modest improvements in this type of ground-based radar system, in particular better sky coverage, should allow for the detection of multiple examples of each type of source. An alternate possibility is to piggyback on already existing radar employed in DEW systems.

We are grateful to W. J. Baggaley, B. T. Draine, C. D. Matzner, D. D. Meisel, R. E. Pudritz, and D. N. Spergel for helpful discussions. This research was supported by NSERC of Canada and the Canada Research Chair program and has made use of the SIMBAD database, operated at CDS, Strasbourg, France, and of NASA's Astrophysics Data System.

APPENDIX

In this appendix we rederive some of the relations used in § 2, employing the classical theory of meteors. In the meteoroid frame, the air flow has a kinetic energy flux

$$F = \tfrac{1}{2}\rho_a v^3. \tag{A1}$$

Following the meteoritics literature, we define a shape factor A to be the ratio of the area A_m of the meteoroid divided by the two-thirds power of the volume (m/ρ), or

$$A \equiv \frac{A_m}{(m/\rho)^{2/3}}. \tag{A2}$$

For a sphere, $A = (9\pi/16)^{1/3} \approx 1.2$. The kinetic luminosity seen by the meteoroid is then $A_m F = (A/2)(m/\rho)^{2/3}\rho_a v^3$; assume that a fraction Λ of this kinetic luminosity goes toward ablating the meteor. Then the time rate of change of the binding energy is

$$\frac{dE}{dt} = -\frac{\Lambda A}{2}\left(\frac{m}{\rho}\right)^{2/3}\rho_a v^3. \tag{A3}$$

Typical estimates for Λ are around 0.5. It follows that the rate of ablation is

$$\frac{dm}{dt} = -\frac{\Lambda A}{2\zeta}\left(\frac{m}{\rho}\right)^{2/3}\rho_a v^3, \tag{A4}$$

where, the reader will recall, the binding energy E is related to the meteoroid mass m by the heat of ablation ζ, $E = \zeta m$. From equation (8), the number of ions produced per centimeter along the path is

$$q = -\frac{\beta}{v\mu}\frac{dm}{dt}, \tag{A5}$$

where μ is the mean molecular weight of the meteoroid (recall that β is the number of ions produced by each meteoroid atom). Combining this with equation (A4), we find

$$q = \beta\frac{\Lambda A}{2\zeta\mu}\left(\frac{m}{\rho}\right)^{2/3}\rho_a v^2. \tag{A6}$$

This is known as the ionization equation.

The maximum line density along the track can be found by differentiating the ionization equation with respect to time:

$$\frac{1}{q}\frac{dq}{dt} = \frac{1}{\beta}\frac{d\beta(v)}{dt} + \frac{2}{3m}\frac{dm}{dt} + \frac{1}{\rho_a}\frac{d\rho_a}{dt} + \frac{2}{v}\frac{dv}{dt}. \tag{A7}$$

Note that $\beta(v) \propto v^n$, so that both the first and last terms on the right-hand side are proportional to

$$\frac{1}{v}\frac{dv}{dt}. \tag{A8}$$

We assume for the moment that this is smaller than either the mass or density variations. Then the maximum value of q occurs when

$$\frac{2}{3m}\frac{dm}{dt} = -\frac{1}{\rho_a}\frac{d\rho_a}{dt}, \tag{A9}$$

or

$$\frac{2}{3m}\left(-\frac{q_{\max}\mu}{\beta}v\right) = -\frac{v}{H_p}, \tag{A10}$$

where H_p is the density scale height. Thus,

$$q_{\max} = \frac{3}{2}\frac{\beta m}{\mu H_p}. \tag{A11}$$

In words, the maximum line density is given by spreading the meteoroid over approximately a scale height and accounting for the number β of atoms that are ionized for each atom in the meteoroid.

Next we justify the neglect of terms proportional to the derivative of the velocity. The momentum equation for the meteoroid is

$$m\frac{dv}{dt} = mg - C_D A\left(\frac{m}{\rho}\right)^{2/3}\rho_a v^2, \tag{A12}$$

where C_D is the drag coefficient. The mean free path at meteor heights is of order 10 cm, much larger than the typical radius of the meteoroids we are interested in. In that case $C_D = 1$. The velocity derivative becomes

$$\frac{1}{v}\frac{dv}{dt} = \frac{g}{v} - A\left(\frac{m}{\rho}\right)^{2/3}\frac{\rho_a v}{m}. \tag{A13}$$

We note that $H_p \approx c^2/g$, where c is the sound speed; then

$$\frac{v}{H_p} \approx \left(\frac{v}{c}\right)^2 \frac{g}{v} \gg \frac{g}{v}, \tag{A14}$$

so that the first term on the right-hand side of equation (A13) is negligible compared to v/H_p; recall that the meteoroids are highly supersonic. Next we compare the velocity gradient in equation (A7) (including only the second term on the right-hand side of eq. [A13]),

$$\frac{2+n}{v}\frac{dv}{dt} \approx A\left(\frac{m}{\rho}\right)^{2/3}\frac{\rho_a v}{m} \sim \frac{a^2\rho_a v}{\rho a^3} \sim \frac{\rho_a}{\rho}\frac{H_p}{a}\frac{v}{H_p}, \tag{A15}$$

to

$$\frac{2}{3m}\frac{dm}{dt} = -\frac{\Lambda A}{2\zeta}\left(\frac{m}{\rho}\right)^{2/3}\frac{\rho_a v^3}{m}. \tag{A16}$$

The ratio is

$$\frac{12}{\Lambda}\frac{\zeta}{v^2} = \frac{3}{2}\left(\frac{\zeta}{2\times 10^{11}\ \mathrm{cm^2\ s^{-2}}}\right)\left(\frac{v}{40\ \mathrm{km\ s^{-1}}}\right)^2\left(\frac{10^{-1}}{\Lambda}\right), \tag{A17}$$

where we took $n = 2$.

McKinley gives estimates for Λ that are of order unity. For these values, the velocity derivative is much smaller than the mass derivative. We conclude that the logarithmic mass derivative is comparable to or larger than the logarithmic velocity derivative.

REFERENCES

Aumann, H. H., et al. 1984, ApJ, 278, L23
Backman, D. E., & Paresce, F. 1993, in Protostars and Planets III, ed. E. H. Levy & J. I. Lunine (Tucson: Univ. Arizona Press), 1253
Baggaley, W. J. 2000, J. Geophys. Res., 105, 10353
Baggaley, W. J., Bennett, R. G. T., Steel, D. I., & Taylor, A. D. 1994, QJRAS, 35, 293
Beck-Winchatz, B., Böhm, K.-H., & Noriega-Crespo, A. 1996, AJ, 111, 346
Binney, J., & Tremaine, S. 1987, Galactic Dynamics (Princeton: Princeton Univ. Press)
Böhm, K.-H., & Matt, S. 2001, PASP, 113, 158
Bronshten, V. A. 1983, Physics of Meteoric Phenomena (Dordrecht: Reidel)
Campbell-Brown, M., & Jones, J. 2003, MNRAS, 343, 775
Chugai, N. N. 2001, Sol. Syst. Res., 35, 307
Crifo, F., Vidal-Madjar, A., Lallement, R., Ferlet, R., & Gerbaldi, M. 1997, A&A, 320, L29
Dehnen, W., & Binney, J. J. 1998, MNRAS, 298, 387
de Zeeuw, P. T., Hoogerwerf, R., de Bruijne, J. H. J., Brown, A. G. A., & Blaauw, A. 2001, Encyclopedia of Astronomy and Astrophysics (Bristol: Institute of Physics Publ.)
Dohnanyi, J. S. 1969, J. Geophys. Res., 74, 2531
Draine, B. T., & Salpeter, E. E. 1979, ApJ, 231, 77
Eislöffel, J., Mundt, R., Ray, T. P., & Rodríguez, L. F. 2000, in Protostars and Planets IV, ed. V. Mannings, A. P. Boss, & S. S. Russell (Tucson: Univ. Arizona Press), 815
Fowler, R. H., & Nordheim, L. 1928, Proc. R. Soc. London A, 119, 173
Frisch, P. C., et al. 1999, ApJ, 525, 492
Gillett, F. C. 1986, in Light on Dark Matter, ed. F. P. Israel (Dordrecht: Reidel), 61
Gilmore, G., & Reid, N. 1983, MNRAS, 202, 1025
Groenewegen, M. A. T. 1997, A&A, 317, 503
Guillout, P., Sterzik, M. F., Schmitt, J. H. M. M., Motch, C., & Neuhäuser, R. 1998, A&A, 337, 113
Habing, H. J. 1996, A&A Rev., 7, 97
Heiles, C. 1998, in The Local Bubble and Beyond, ed. D. Breitschwerdt, M. J. Freyberg, & J. Trümper (Berlin: Springer), 229
Herczeg, G. J., Linsky, J. L., Valenti, J. A., Johns-Krull, C. M., & Wood, B. E. 2002, ApJ, 572, 310
Holland, W. S., et al. 1998, Nature, 392, 788
Hollenbach, D. J., Yorke, H. W., & Johnstone, D. 2000, in Protostars and Planets IV, ed. V. Mannings, A. P. Boss, & S. S. Russell (Tucson: Univ. Arizona Press), 401
Ivezić, Ž., et al. 2001, AJ, 122, 2749
Jackson, T., Ivezić, Ž., & Knapp, G. R. 2002, MNRAS, 337, 749
Janches, D., Mathews, J. D., Meisel, D. D., & Zhou, Q.-H. 2000, Icarus, 145, 53
Jones, A. P., Tielens, A. G. G. M., & Hollenbach, D. J. 1996, ApJ, 469, 740
Jones, W. 1997, MNRAS, 288, 995
Jones, W., & Halliday, I. 2001, MNRAS, 320, 417
Jura, M. 1996, ApJ, 472, 806
Jura, M., Chen, C., & Werner, M. W. 2000, ApJ, 541, 264
Jura, M., Turner, J., & Balm, S. P. 1997, ApJ, 474, 741
Jura, M., Webb, R. A., & Kahane, C. 2001, ApJ, 550, L71
Kim, S., & Martin, P. G. 1995, ApJ, 444, 293
Königl, A., & Pudritz, R. E. 2000, in Protostars and Planets IV, ed. V. Mannings, A. P. Boss, & S. S. Russell (Tucson: Univ. Arizona Press), 759
Krivova, N. A., & Solanki, S. K. 2003, A&A, 402, L5
Krüger, D., & Sedlmayr, E. 1997, A&A, 321, 557
Lagrange, A.-M., Backman, D. E., & Artymowicz, P. 2000, in Protostars and Planets IV, ed. V. Mannings, A. P. Boss, & S. S. Russell (Tucson: Univ. Arizona Press), 639
Landgraf, M., Baggaley, W. J., Grün, E., Krüger, H., & Linkert, G. 2000, J. Geophys. Res., 105, 10343
Levison, H. F., & Duncan, M. J. 1994, Icarus, 108, 18
Li, A., & Draine, B. T. 2001, ApJ, 554, 778
Li, A., & Greenberg, J. M. 1998, A&A, 331, 291
Makarov, V. V., & Fabricius, C. 2001, A&A, 368, 866
Manning, L. A. 1958, J. Geophys. Res., 63, 181
Mathews, J. D., Meisel, D. D., Hunter, K. P., Getman, V. S., & Zhou, Q. 1997, Icarus, 126, 157
Mathis, J. S., Mezger, P. G., & Panagia, N. 1983, A&A, 128, 212
Mathis, J. S., Rumpl, W., & Nordsieck, K. H. 1977, ApJ, 217, 425
McKinley, D. W. R. 1961, Meteor Science and Engineering (New York: McGraw-Hill)
Meisel, D. D., Janches, D., & Mathews, J. D. 2002a, ApJ, 567, 323
———. 2002b, ApJ, 579, 895
Mezger, P. G., Mathis, J. S., & Panagia, N. 1982, A&A, 105, 372
Molster, F. J., Yamamura, I., Waters, L. B. F. M., Nyman, L.-Å., Käufl, H.-U., de Jong, T., & Loup, C. 2001, A&A, 366, 923
Mouri, H., & Taniguchi, Y. 2000, ApJ, 534, L63
Murray, C. D., & Dermott, S. F. 1999, Solar System Dynamics (Cambridge: Cambridge Univ. Press)
Öpik, E. J. 1976, Interplanetary Encounters: Close-Range Gravitational Interactions (New York: Elsevier)
Pöppel, W. 1997, Fundam. Cosmic Phys., 18, 1
Reipurth, B., & Bally, J. 2001, ARA&A, 39, 403
Richer, J. S., Shepherd, D. S., Cabrit, S., Bachiller, R., & Churchwell, E. 2000, in Protostars and Planets IV, ed. V. Mannings, A. P. Boss, & S. S. Russell (Tucson: Univ. Arizona Press), 867
Robichon, N., Arenou, F., Mermilliod, J.-C., & Turon, C. 1999, A&A, 345, 471
Schneider, G., et al. 1999, ApJ, 513, L127

Scholl, H., Roques, F., & Sicardy, B. 1993, Celest. Mech. Dyn. Astron., 56, 381
Sfeir, D. M., Lallement, R., Crifo, F., & Welsh, B. Y. 1999, A&A, 346, 785
Shu, F. H., Najita, J. R., Shang, H., & Li, Z.-Y. 2000, in Protostars and Planets IV, ed. V. Mannings, A. P. Boss, & S. S. Russell (Tucson: Univ. Arizona Press), 789
Smith, B. A., & Terrile, R. J. 1984, Science, 226, 1421
Spangler, C., Sargent, A. I., Silverstone, M. D., Becklin, E. E., & Zuckerman, B. 2001, ApJ, 555, 932
Stelzer, B., & Neuhäuser, R. 2000, A&A, 361, 581
Taylor, A. D., Baggaley, W. J., & Steel, D. I. 1996, Nature, 380, 323
Tielens, A. G. G. M., McKee, C. F., Seab, C. G., & Hollenbach, D. J. 1994, ApJ, 431, 321
Torra, J., Fernández, D., & Figueras, F. 2000, A&A, 359, 82
Weingartner, J. C., & Draine, B. T. 2001a, ApJ, 548, 296
———. 2001b, ApJ, 553, 581
Weingartner, J. C., & Draine, B. T. 2001c, ApJS, 134, 263
Whittet, D. C. B. 1992, Dust in the Galactic Environment (Bristol: Institute of Physics Publ.)
Wilner, D. J., Ho, P. T. P., Kastner, J. H., & Rodríguez, L. F. 2000, ApJ, 534, L101
Wilner, D. J., Holman, M. J., Kuchner, M. J., & Ho, P. T. P. 2002, ApJ, 569, L115
Wisdom, J., & Holman, M. 1991, AJ, 102, 1528
Zinner, E. 1998, Annu. Rev. Earth Planet. Sci., 26, 147
Zuckerman, B. 2001, ARA&A, 39, 549
Zuckerman, B., & Becklin, E. E. 1993, ApJ, 414, 793
Zuckerman, B., Song, I., Bessell, M. S., & Webb, R. A. 2001a, ApJ, 562, L87
Zuckerman, B., Song, I., & Webb, R. A. 2001b, ApJ, 559, 388
Zuckerman, B., & Webb, R. A. 2000, ApJ, 535, 959